LPSC14081
UCD-2014-03

Constraints on and future prospects for Two-Higgs-Doublet Models in light of the LHC Higgs signal

Béranger Dumont[1],* John F. Gunion[2],† Yun Jiang[2],‡ and Sabine Kraml[1§]

(1) Laboratoire de Physique Subatomique et de Cosmologie,

Université Grenoble-Alpes, CNRS/IN2P3,

53 Avenue des Martyrs, F-38026 Grenoble, France and

(2) Department of Physics, University of California, Davis, CA 95616, USA

arXiv:1405.3584v2 [hep-ph] 24 Jan 2015

We analyze the Two-Higgs-Doublet Models (2HDMs) of Type I and Type II for consistency with the latest measurements of the ~ 125.5 GeV Higgs-like signal at the LHC. To this end, we perform scans of the 2HDM parameter space taking into account all relevant pre-LHC constraints as well as the most recent limits coming from searches for heavy Higgs-like states at the LHC. The current status of the 2HDMs of Type I and Type II is discussed assuming that the observed 125.5 GeV state is one of the two CP-even Higgs bosons, either the lighter h or the heavier H. Implications for future experiments, including expectations regarding other lighter or heavier Higgs bosons are given. The possible importance of heavier Higgs bosons feeding the signals for the 125.5 GeV state is also evaluated.

PACS numbers: 12.60.Fr, 14.80.Ec, 14.80.Fd

Keywords: Higgs physics, 2-Higgs-Doublet Model, LHC

*dumont@lpsc.in2p3.fr

†jfgunion@ucdavis.edu

‡yunjiang@ucdavis.edu

§sabine.kraml@lpsc.in2p3.fr

I. INTRODUCTION

Following the discovery by the ATLAS and CMS experiments at the LHC [1, 2] of a Higgs-like particle, additional measurements of its properties using the full data sets at $\sqrt{s} = 7$ and 8 TeV reveal that the observed state with a mass near 125.5 GeV is quite Standard Model (SM)-like [3–5]. It is thus clear that models with an extended Higgs sector will be significantly constrained by the data.

In particular, it is interesting to consider the simplest such extensions of the SM, namely Two-Higgs-Doublet Models (2HDMs). For comprehensive reviews see, *e.g.*, [6–8]. These models have attracted a lot of attention recently. A large number of papers [9–18] performed fits of current data for the 125.5 GeV Higgs-like state (as per the status post Moriond 2013) within the context of 2HDMs, and investigated the consequent phenomenology of the other Higgs states present in the models. Among these papers, [10, 11, 13] consider 2HDMs with a conserved Z_2 symmetry, [15, 16, 19, 20] focus on the case of an aligned 2HDM, [14, 18] investigate the possibility of CP-violation in the Higgs sector, and [17] concentrates on the question of the triple-Higgs coupling. The general conditions for the alignment limit, in which the lightest CP-even Higgs boson of a 2HDM mimics the Standard Model Higgs, without decoupling the other scalars were studied in [21]. Moreover, the prospects for future LHC running and/or for other future colliders in view of the current data were investigated in [19, 20, 22–24]. The possibility of CP violation in 2HDMs also implies an important link of such models to electroweak baryogenesis, a topic that was revisited recently in [25–28].

The present work goes beyond what was done in the above-referenced studies of 2HDMs in that we provide a very comprehensive and complete analysis of the status of the CP-conserving 2HDMs of Type I and Type II, considering both the cases where the observed Higgs particle at the LHC is the lighter CP-even state h or the heavier CP-even state H. [1] (The possibility of the heavier H being identified with the 125.5 GeV state was also considered in [11, 13, 16, 23, 24].) In particular, we employ all the latest results for the signal strength measurements from LHC8, include a consistent treatment of feed down (FD) from the production of heavier Higgs states, and discuss the prospects for LHC14.

[1] Given that the observed state clearly has ZZ, WW couplings that are not far from SM-like, it cannot be identified with the A which has no VV tree-level couplings. In this paper, we also do not consider cases in which the observed state is a mixture of two or more nearly degenerate 2HDM states.

In scanning the 2HDM parameter space, we use the parameter set consisting of the physical Higgs masses, m_h, m_H, $m_{H^\pm}$ and m_A, the Z_2 soft-breaking parameter m_{12}, the CP-even Higgs mixing parameter α and the ratio of the two vacuum expectation values $\tan\beta = v_2/v_1$. We impose all relevant constraints from precision electroweak data, from stability, unitarity and perturbativity of the potential, as well as from B physics and from the direct searches at LEP. For this we closely follow the approach of [29]. Points are retained only when these "preLHC" constraints are all satisfied. Once the preLHC constraints have been applied, we require that the rates for channels involving heavier Higgs bosons all lie below the existing 95% confidence level (C.L.) limits coming from the LHC.

The next step, and the most important one for this work, is to impose the restrictions on the 2HDM parameter space from the measured Higgs signal. The Higgs measurements are conventionally phrased in terms of "signal strengths", *i.e.* the ratios to the SM predictions for different production channels, X, and different decay modes, Y,

$$\mu_X(Y) = \frac{\sigma(X)\mathrm{BR}(Y)}{\sigma_{\mathrm{SM}}(X)\mathrm{BR}_{\mathrm{SM}}(Y)}\,, \tag{1}$$

where the numerator and denominator are evaluated for the same Higgs mass. The production modes for the Higgs boson considered are ggF (gluon fusion, also denoted as gg), VBF (vector boson fusion), ttH (associated production with $t\bar{t}$) and VH (associated production with a vector boson). The relevant decay modes are those into $Y = \gamma\gamma, VV, b\bar{b}$, and $\tau\tau$ (where $VV \equiv ZZ, WW$). In practice, we employ the signal strength likelihoods in the $\mu_{\mathrm{ggF+ttH}}$ versus $\mu_{\mathrm{VBF+VH}}$ planes for each of the final states Y as determined in [30], combining all publicly available information from ATLAS and CMS.[2] The $[\mu_{\mathrm{ggF+ttH}}, \mu_{\mathrm{VBF+VH}}]$ approach has been systematically adopted by the experimental collaborations. It has the advantage of taking into account correlations not accounted for when individual $X \to H \to Y$ channels are treated separately. We will require that the Higgs rates for all channels fall within the 95% C.L. regions in the $[\mu_{\mathrm{ggF+ttH}}, \mu_{\mathrm{VBF+VH}}]$ plane. Points which satisfy the preLHC constraints, the heavy Higgs limits and the Higgs fitting constraints will be labelled

[2] Combining VBF and VH is motivated in models where the couplings of the Higgs to WW and to ZZ are scaled equally, as is the case in any 2HDM because of custodial symmetry. Combining ggF and ttH is more a matter of convenience, partially motivated by the fact that the current LHC measurements do not probe ggF and ttH in any given final state at the same time: $H \to b\bar{b}$ is probed via ttH, not ggF, whereas all the other final states are probed quite precisely via ggF and with much poorer precision via ttH.

as "postLHC8" points.

There is a further issue arising from the fact that there are various ways in which the 125.5 GeV Higgs boson can be produced as a result of feed down from the production of heavier states – in the case of $m_h = 125.5$ GeV this includes the $H, A, H^\pm$ [31] while if $m_H = 125.5$ GeV only the A and $H^\pm$ can feed the 125.5 GeV signal. If such FD processes occur at a significant rate, the fit to the Higgs measurements using only direct h or H production processes may no longer be valid. For most of our plots, we will show only those postLHC8 points for which the production rate from FD will not distort the fits to the 125.5 GeV resonance. Such points are called "FDOK." The detailed feed down limits employed for a point to be FDOK will be given later. These FD processes may be tested by a variety of means. For example, for the important FD sources of $A \to Zh$ and $H \to hh$, the final state mass can be reconstructed and m_A and m_H will be determined should the rates be significant; see the current limits from CMS in [32]. Then, data points lying within the relevant mass windows can be separated off. For the $H \to hh$ case, the decay products from the second h are visible for most h decays and events with this extra final state "activity" can be separated off. More complicated FD chains will have even more extra particles and constraints that will allow their separation. Feed down must also be considered in the $m_H = 125.5$ GeV case — the process $gg \to A \to ZH$ adds events to the ZH final state beyond those from $Z^* \to ZH$; we will comment on this possibility in Section IV.

The rest of the paper is organized as follows. In Section II we give details on the scan ranges and the constraints incorporated. The case of the lighter CP-even Higgs h being the observed state near 125.5 GeV is discussed in Section III, and the case of the heavier CP-even Higgs H in Section IV. Section V contains our conclusions. Details on the feed down of a heavier Higgs to the 125.5 GeV state are discussed in Appendix A. Appendix B gives details regarding the nondecoupling charged-Higgs contributions to the Higgs-$\gamma\gamma$ coupling and the relationship to wrong-sign Higgs Yukawa couplings for down-type quarks.

II. PROCEDURAL DETAILS

In this section we provide some details regarding the parameter scans, the fitting of the signal strengths, and the incorporation of limits related to the Higgs bosons that are heavier than the 125.5 GeV state.

	Type I and Type II	Type I		Type II	
Higgs	C_V	C_U	C_D	C_U	C_D
h	$\sin(\beta-\alpha)$	$\cos\alpha/\sin\beta$	$\cos\alpha/\sin\beta$	$\cos\alpha/\sin\beta$	$-\sin\alpha/\cos\beta$
H	$\cos(\beta-\alpha)$	$\sin\alpha/\sin\beta$	$\sin\alpha/\sin\beta$	$\sin\alpha/\sin\beta$	$\cos\alpha/\cos\beta$
A	0	$\cot\beta$	$-\cot\beta$	$\cot\beta$	$\tan\beta$

TABLE I: Tree-level vector boson couplings C_V ($V = W, Z$) and fermionic couplings C_F ($F = U, D$) normalized to their SM values for the Type I and Type II 2HDMs.

A. Scan ranges and procedures

As in [29], we employ a modified version of the code `2HDMC` [33, 34] for our numerical calculations. All relevant contributions to loop-induced processes are taken into account, in particular those with heavy quarks (t and b), $W^\pm$ and $H^\pm$. A number of different input sets can be used in the `2HDMC` context. We have chosen to use the "physical basis" in which the inputs are the physical Higgs masses ($m_h, m_H, m_A, m_{H^\pm}$), the vacuum expectation value ratio ($\tan\beta$), and the CP-even Higgs mixing angle, α, supplemented by m_{12}^2. The additional parameters λ_6 and λ_7 are assumed to be zero as a result of a Z_2 symmetry being imposed on the dimension-4 operators under which $H_1 \to H_1$ and $H_2 \to -H_2$. $m_{12}^2 \neq 0$ is allowed as a "soft" breaking of the Z_2 symmetry. With the above inputs, $\lambda_{1,2,3,4,5}$ as well as m_{11}^2 and m_{22}^2 are determined (the latter two via the minimization conditions for a minimum of the vacuum) [7]. We scan over the following ranges:[3]

$$\alpha \in [-\pi/2, +\pi/2]\,, \quad \tan\beta \in [0.5, 60]\,, \quad m_{12}^2 \in [-(2\text{ TeV})^2, (2\text{ TeV})^2]\,,$$
$$m_A \in [5\text{ GeV}, 2\text{ TeV}]\,, \quad m_{H^\pm} \in [m^*, 2\text{ TeV}]\,, \tag{2}$$

where m^* is the lowest value of $m_{H^\pm}$ allowed by LEP direct production limits and B physics constraints. The LEP limits on the $H^\pm$ are satisfied by requiring $m_{H^\pm} \geq 90$ GeV. The lower bounds from B physics are shown as a function of $\tan\beta$ in Fig. 15 of [8] in the case of the Type II model (roughly $m^* \sim 300$ GeV in this case) and in Fig. 18 of [8] in the case of the

[3] The upper and lower bounds on $\tan\beta$ are chosen to ensure that the bottom and top Yukawa couplings, respectively, lie within the perturbative region. Unlike the Z_2 symmetric 2HDM which constrains $\tan\beta \lesssim 7$ [22], high $\tan\beta$ values are allowed when the Z_2 symmetry is softly broken. A safe upper limit, as adopted here, is $\tan\beta \leq 60$.

Type I model.

The couplings, normalized to their SM values, of the Higgs bosons to vector bosons (C_V) and to up- and down-type fermions (C_U and C_D) are functions of α and β as given in Table I; see *e.g.* [6] for details. The Type I and Type II models are distinguished only by the pattern of their fermionic couplings. We note that the range of α employed guarantees that the top quark Yukawa coupling is always positive in our convention. For the most part, in particular for the case of $m_h \sim 125.5$ GeV, one also finds that $\sin(\beta - \alpha) > 0$.

For the remaining physical Higgs masses, we consider

$$m_h \in [123\ \text{GeV}, 128\ \text{GeV}]\,, \quad m_H \in\,]128\ \text{GeV}, 2\ \text{TeV}]\,, \tag{3}$$

for the case that h is the observed state near 125.5 GeV, or

$$m_H \in [123\ \text{GeV}, 128\ \text{GeV}]\,, \quad m_h \in [10\ \text{GeV}, 123\ \text{GeV}[\,, \tag{4}$$

for the case that H is the observed state near 125.5 GeV. The window of 125.5 ± 2.5 GeV is adopted to account for theoretical uncertainties. However, we do not consider the cases where the A and/or the other CP-even Higgs are close to 125.5 GeV and possibly contribute to the observed signal. Thus, for $m_h \sim 125.5$ GeV ($m_H \sim 125.5$ GeV) we require that m_H (m_h) and m_A not be within the $[123, 128]$ GeV window nor within a $m_h \pm 4$ GeV ($m_H \pm 4$ GeV) mass window where m_h (m_H) is the particular mass value generated within the $[123, 128]$ GeV range.

We should note that our scans were performed in a manner that provides adequate point density in all regions of the various plots and predictions of interest. This means that, besides very broad (usually flat) scans in the input parameters mentioned above, we also used scans designed to focus on "hard-to-reach" regions of parameter space of particular interest and importance.

B. Limits imposed by nonobservation of Higgs bosons other than the 125.5 GeV state

As noted in the Introduction, it is necessary to take into account LHC exclusion limits for Higgs bosons that are heavier than 125.5 GeV. In the case that the h is identified with the ~ 125.5 GeV state the relevant channels are $gg \to H \to 4\ell, 2\ell 2\nu$, $gg \to H, A \to \tau\tau$ and

$gg \to b\bar{b}H, b\bar{b}A \to b\bar{b}\tau\tau$ at the LHC. When these limits have been applied the points will be denoted by the phrase "H/A limits." In the case that $m_H \sim 125.5$ GeV is assumed, the only LHC limits that apply are those on $gg \to A \to \tau\tau$ and $gg \to b\bar{b}A \to b\bar{b}\tau\tau$. Points that remain acceptable are denoted by "A limits". Direct search limits on the $H^\pm$ at the LHC do not impact the parameter space once the B physics limits described below are imposed. In addition, the impact of the CMS search for $H \to hh$ and $A \to Zh$ [32] and its relation with FD will be discussed in Sections III B and C.

For $H/A \to \tau\tau$, we employ the recent CMS limits based on the 8 TeV data [35], which are presented separately for the bbH ($b\bar{b}$ associated production of the Higgs) and ggF production modes. In taking these limits into account, it will be important to note that in Type II models the coupling of the H and A to down-type fermions can be dramatically enhanced at large $\tan\beta$ compared to the SM expectation and that this enhancement will influence both bbH and ggF production. When m_A and m_H are within 15% of one another, which is the approximate resolution in the invariant mass of a pair of τ leptons, we will add their signals together.

Turning to $H \to ZZ$, we employ the latest ATLAS and CMS searches for heavy Higgs-like states in the $H \to ZZ \to 4\ell$ channel [36, 37] [4] and the CMS search in the $H \to ZZ \to 2\ell 2\nu$ channel [39]. In the context of 2HDMs, there are two important considerations associated with using the limits as presented by the ATLAS and CMS collaborations. First, the VV couplings shown in Table I imply $(C_V^h)^2 + (C_V^H)^2 = 1$ for the coupling strengths relative to the SM Higgs. Thus, if the h is the 125.5 GeV state, the H will have a small coupling to W, Z due to the fact that the h must be very SM-like in order to describe the data at ~ 125.5 GeV, as shown, *e.g.*, in Fig. 10 of [30]. Thus, only ggF production is relevant for H. However, only ATLAS presents constraints on a high mass Higgs arising purely from the ggF initial state with the full statistics at $7+8$ TeV, for $m_H > 200$ GeV [36]. All the other results, *i.e.* (*i*) ATLAS $H \to 4\ell$ for $m_H \in [130, 180]$ GeV, (*ii*) CMS $H \to 4\ell$ and (*iii*) CMS $H \to 2\ell 2\nu$ are implemented in our analysis under the assumption that the experimental search is fully inclusive. The limit is thus rescaled by a factor $\sigma^{\rm tot}_{H_{\rm SM}}/\sigma_{gg\to H_{\rm SM}}$. Second, the width of the H

[4] Note that the CMS results on $H \to ZZ$ are presented after combination of the 4ℓ (where $\ell = e, \mu$) and $2\ell 2\tau$ channels. However, the limit is almost uniquely driven by the 4ℓ channels as can be seen from the result based on $H \to ZZ \to 2\ell 2\tau$ only, which is available as supplementary material on the TWiki page [38].

in the 2HDM can be much smaller than the large SM Higgs widths assumed in the ATLAS and CMS analyses. We correct for the width difference by rescaling the observed limits on $\sigma \times \mathrm{BR}$ by the factor $f = \sqrt{\frac{\Gamma_H^2 + (4\ \mathrm{GeV})^2}{\Gamma_{H_{\mathrm{SM}}}^2 + (4\ \mathrm{GeV})^2}}$, where 4 GeV is the experimental resolution in the 4ℓ final state [40].

C. Constraints from the signal strength measurements at 125.5 GeV

For each scan point that passes the constraints explained above, we compute the predictions for $\mu_{\mathrm{ggF+ttH}}(Y)$ and $\mu_{\mathrm{VBF+VH}}(Y)$ for the main decay modes Y ($\gamma\gamma, VV, b\bar{b}$, and $\tau\tau$) in terms of the reduced couplings C_U, C_D, and C_V, see Table I. To this end, we also need the loop-induced $\gamma\gamma$ and gg couplings of the Higgs boson with mass around 125.5 GeV; for these we employ the full 1-loop amplitudes in `2HDMC` (including the contribution from the charged Higgs bosons in the $\gamma\gamma$ case), where SM contributions are scaled according to the values of C_U, C_D and C_V.

To combine the information provided by ATLAS, CMS and the Tevatron experiments on the $\gamma\gamma$, $ZZ^{(*)}$, $WW^{(*)}$, $b\bar{b}$ and $\tau\tau$ final states including the error correlations among the (VBF+VH) and (ggF+ttH) production modes, we follow the approach of [30]. Concretely, we fit the likelihood from the 68% C.L. contour provided by the experiments for each decay mode Y in the $\mu_{\mathrm{ggF+ttH}}(Y)$ versus $\mu_{\mathrm{VBF+VH}}(Y)$ plane, using a Gaussian approximation. For each experiment, $-2\log L_Y = \chi^2_Y$ can then be expressed as

$$\begin{aligned}
\chi^2_Y &= (\boldsymbol{\mu}_Y - \hat{\boldsymbol{\mu}}_Y)^T \begin{pmatrix} \sigma^2_{\mathrm{ggF},Y} & \rho_Y \sigma_{\mathrm{ggF},Y}\sigma_{\mathrm{VBF},Y} \\ \rho_Y \sigma_{\mathrm{ggF},Y}\sigma_{\mathrm{VBF},Y} & \sigma^2_{\mathrm{VBF},Y} \end{pmatrix}^{-1} (\boldsymbol{\mu}_Y - \hat{\boldsymbol{\mu}}_Y) \qquad (5) \\
&= (\boldsymbol{\mu}_Y - \hat{\boldsymbol{\mu}}_Y)^T \begin{pmatrix} a_Y & b_Y \\ b_Y & c_Y \end{pmatrix} (\boldsymbol{\mu}_Y - \hat{\boldsymbol{\mu}}_Y) \\
&= a_Y(\mu_{\mathrm{ggF},Y} - \hat{\mu}_{\mathrm{ggF},Y})^2 + 2b_Y(\mu_{\mathrm{ggF},Y} - \hat{\mu}_{\mathrm{ggF},Y})(\mu_{\mathrm{VBF},Y} - \hat{\mu}_{\mathrm{VBF},Y}) + c_Y(\mu_{\mathrm{VBF},Y} - \hat{\mu}_{\mathrm{VBF},Y})^2 \,,
\end{aligned}$$

where the indices ggF and VBF stand for (ggF+ttH) and (VBF+VH), respectively, and $\hat{\mu}_{\mathrm{ggF},Y}$ and $\hat{\mu}_{\mathrm{VBF},Y}$ denote the best-fit points obtained from the measurements [30]. The two-dimensional (2D) covariance matrix is explicitly shown in the first line of Eq. (5), with ρ_Y corresponding to the correlation between the measurement of (ggF+ttH) and (VBF+VH). From a digitized version of the 68% C.L. contour, it is possible to fit simultaneously the

parameters a_Y, b_Y, c_Y, $\hat{\mu}_{\mathrm{ggF},Y}$ and $\hat{\mu}_{\mathrm{VBF},Y}$. A combination of ATLAS and CMS can then be made for each decay mode Y and expressed again in terms of a_Y, b_Y, c_Y, $\hat{\mu}_{\mathrm{ggF},Y}$ and $\hat{\mu}_{\mathrm{VBF},Y}$.

Adding up the individual χ^2_Y, we thus obtain a "combined likelihood," which can be used in a simple, generic way to constrain nonstandard Higgs sectors and new contributions to the loop-induced processes, provided they have the same Lagrangian structure as the SM. In this paper, for each scan point that passes the constraints of Sections II A and II B, we demand that each χ^2_Y (for ATLAS and CMS combined) be smaller than 6.18, which corresponds to 95% C.L. in two dimensions. These points are labelled as "postLHC8."

III. $m_h \sim 125.5$ GeV SCENARIOS

In this section we focus on the case that the observed ~ 125.5 GeV state is the h.

A. Current constraints

To cover the case $m_h = 125.5 \pm 2.5$ GeV, we scan over m_H, m_A and $m_{H^\pm}$ as discussed earlier in section II. As regards Yukawa couplings, the scan range of $|\alpha| \leq \pi/2$ implies that $C_U^h = C_D^h > 0$ for Type I, whereas for Type II $C_D^h < 0$ is possible when $\sin\alpha > 0$. Note that with this scanning range for α, $\sin(\beta-\alpha) < 0$ is in principle possible, but is excluded by LHC data in the case of $m_h = 125.5$ GeV. Thus, for both Type I and Type II models, C_V^h and C_U^h are always positive.

As regards the possibilities for $\sin\alpha$, which determines the sign of C_D^h in Type II, there are important constraints from perturbativity of the quartic Higgs couplings (even in the case of the Type I model). Often the strongest constraint is associated with the λ_{AAAA} quartic coupling of four A Higgs bosons. Figure 1 shows the values of λ_{AAAA} that arise after the preLHC conditions listed in the Introduction are satisfied. From the figure we see that perturbativity of this quartic coupling creates a boundary of maximal $\sin(\beta-\alpha)$ values for $\sin\alpha > 0$ and of minimal $\sin(\beta-\alpha)$ values for $\sin\alpha \lesssim -0.3$. The other boundaries arise as a result of constraining other quartic couplings to their perturbative domain. Note in particular that in both Type I and Type II the maximal value of $\sin(\beta-\alpha)$ decreases as $\sin\alpha$ increases starting from $\sin\alpha \sim 0$, whereas $\sin(\beta-\alpha) \sim 1$ is possible for a broad range of $\sin\alpha < 0$ values. This will impact many phenomenological results. In particular, even though the $gg \to h$ fusion production rate is insensitive (not very sensitive) to the sign of $\sin\alpha$ for Type I (Type II), the $\gamma\gamma$ partial width is – as $\sin(\beta-\alpha)$ declines, the W-loop contribution to the $h\gamma\gamma$ coupling decreases, resulting in a decrease in $\mathrm{BR}(h \to \gamma\gamma)$. Hence, the rate for $gg \to h \to \gamma\gamma$ quickly falls below the level acceptable for LHC precision Higgs results. This is also the case for $H \to WW^*$ originating from VBF or VH: while probed with poorer precision, the $\sin(\beta-\alpha)$ factor associated with the HVV vertex is present in both production and decay.

Let us now turn to the constraints on the model parameter space that originate from requiring that the signal strengths of the observed Higgs are matched at 95% C.L. in each

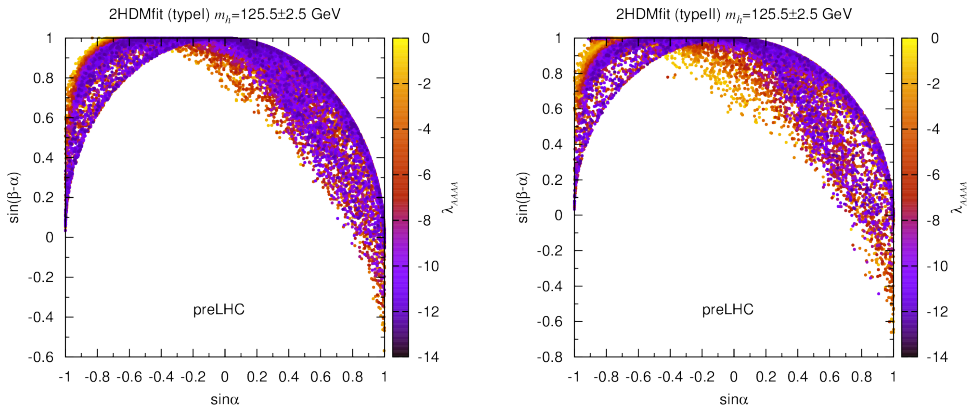

FIG. 1: Values for the quartic coupling λ_{AAAA} for 2HDMs of Type I (left) and Type II (right) in the $\sin(\beta-\alpha)$ versus $\sin\alpha$ plane for $m_h \sim 125.5$ GeV shown as "temperature plots". For all points, the full set of preLHC constraints is satisfied, including all quartic couplings having absolute values below 4π.

final state. We begin with the plots of Fig. 2 showing points in the $\cos(\beta-\alpha)$ vs. $\tan\beta$ plane. Recall that if the h is SM-like, then $\sin(\beta-\alpha)$ will be large and $\cos(\beta-\alpha)$ will be constrained to smaller values. The color scheme is the following:

- grey points are those that survive the preLHC constraints;
- green points are those for which all LHC limits related to the heavier Higgs bosons are obeyed at 95% C.L. — we employ the label "H/A limits" for such points;
- blue points are those for which, *in addition*, the h predictions fall within the 95% C.L. regions in the $[\mu_{\rm ggF+ttH}, \mu_{\rm VBF+VH}]$ plane for *all* final state channels ($\gamma\gamma, VV, b\bar{b}$, and $\tau\tau$) — we term points at this level postLHC8 — *and* in addition the effects of feed down on the 95% C.L. ellipses is small, which we call "postLHC8-FDOK."

We will discuss FD in more detail later, giving the precise criteria required for a point to be "FDOK". For now, let us note the following features of the plots. Looking at the blue points that survive at the postLHC8-FDOK level, we observe that for $m_h \sim 125.5$ GeV in Type I models $|\cos(\beta-\alpha)|$ cannot be too large, especially if $\tan\beta \sim 1$. In the Type II models, either $|\cos(\beta-\alpha)|$ can be quite close to 0 or it can fall in a second branch where fairly large positive $\cos(\beta-\alpha) \gtrsim 0.3$ is allowed if $\tan\beta \lesssim 7$. It turns out that this branch is associated with $\sin(\beta+\alpha) \approx 1$ and $\sin\alpha > 0$ [for which the b-quark Yukawa coupling has

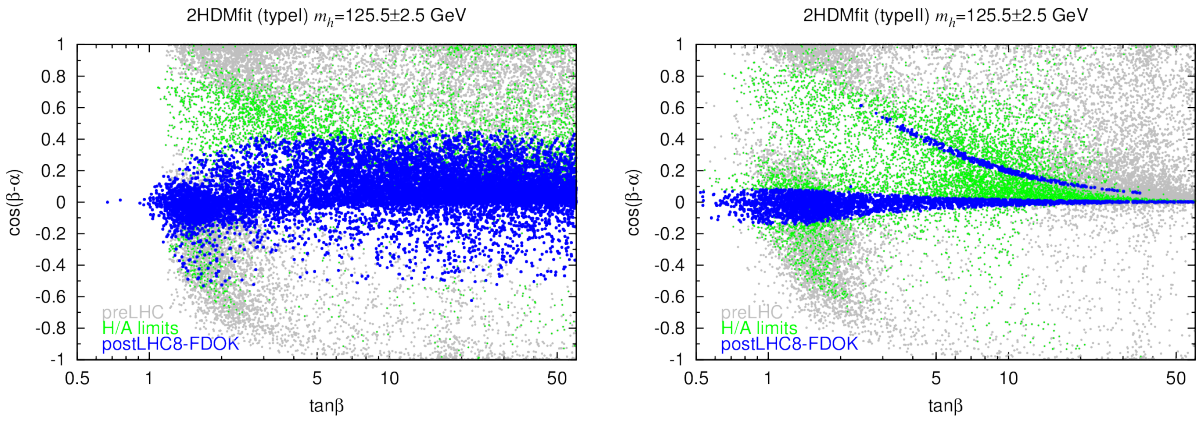

FIG. 2: Constraints in the $\cos(\beta-\alpha)$ versus $\tan\beta$ plane for $m_h \sim 125.5$ GeV. Grey points satisfy preLHC constraints, while green points satisfy in addition the LHC limits on H and A production. Blue points fall moreover within the 7+8 TeV 95% C.L. ellipses in the $[\mu_{\rm ggF+ttH}(Y), \mu_{\rm VBF+VH}(Y)]$ plane for each of the final states considered ($Y = \gamma\gamma, VV, b\bar{b}, \tau\tau$), and the amount of FD from H or A production is small.

the opposite sign relative to the $\sin(\beta-\alpha) \to 1$ limit]. This "wrong-sign" Yukawa coupling, $C_D^h \sim -1$ is the focus of [41].

Insight into the underlying couplings, C_V^h, C_U^h and C_D^h is provided by Fig. 3. There, we see that for both Type I and Type II, $C_V^h \sim +1$ is required for a decent fit to the Higgs data. Further, $C_U^h \sim +1$ is needed in order to describe the observed $\gamma\gamma$ final state rates (*i.e.* a SM-like cancellation between the W and t loops contributing to the $h\gamma\gamma$ coupling is required). In Type I, $C_D^h = C_U^h$ and therefore both must also be close to $+1$. However, this is not required in the Type II models. In fact, the second branch apparent in Fig. 2 corresponds to the $C_D^h \sim -1$ region of the right-hand Type II plot of Fig. 3 — note that the magnitude, $|C_D^h| \sim 1$, is approximately fixed by the need for acceptable fits to the $b\bar{b}$ and $\tau\tau$ final state rates.

Also of interest for the $m_h \sim 125.5$ GeV case is the range of the heavy Higgs masses as a function of $\cos(\beta-\alpha)$, shown in Fig. 4. Clearly, once m_A is above about 800 GeV we are deep into the small $|\cos(\beta-\alpha)|$ decoupling region, whereas for masses below $\sim$ 800 GeV there is considerable spread in the allowed $|\cos(\beta-\alpha)|$ values, in particular in Type I. Thus, if an A (or H or $H^\pm$) is found above $\sim$ 800 GeV, the 2HDMs require that the h is very SM-like, but if m_A is found to be lower in mass, then the h need not be so SM-like. Conversely,

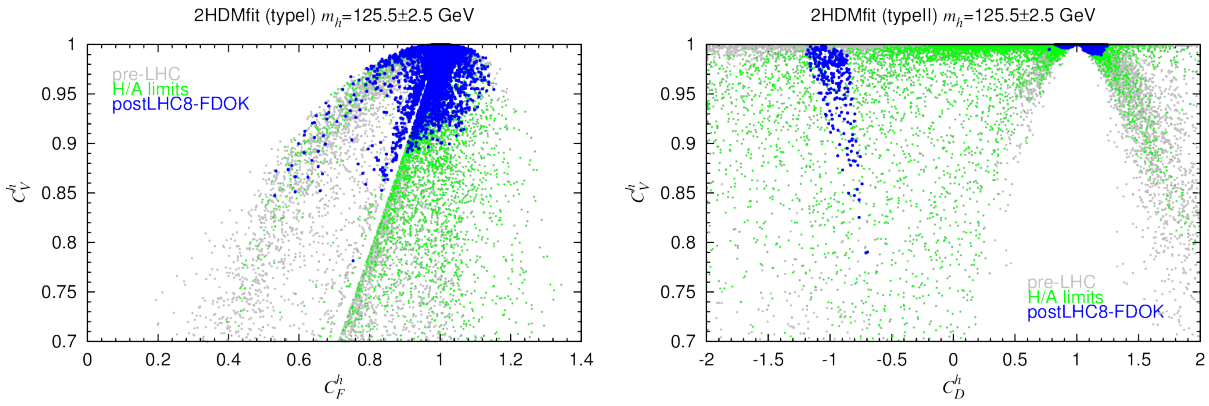

FIG. 3: C_V versus $C_F = C_U = C_D$ for Type I (left) and C_V versus C_D for Type II (right). Color scheme as in Fig. 2. We have restricted the plots to $C_V \geq 0.7$ so as to most clearly display the postLHC8-FDOK points.

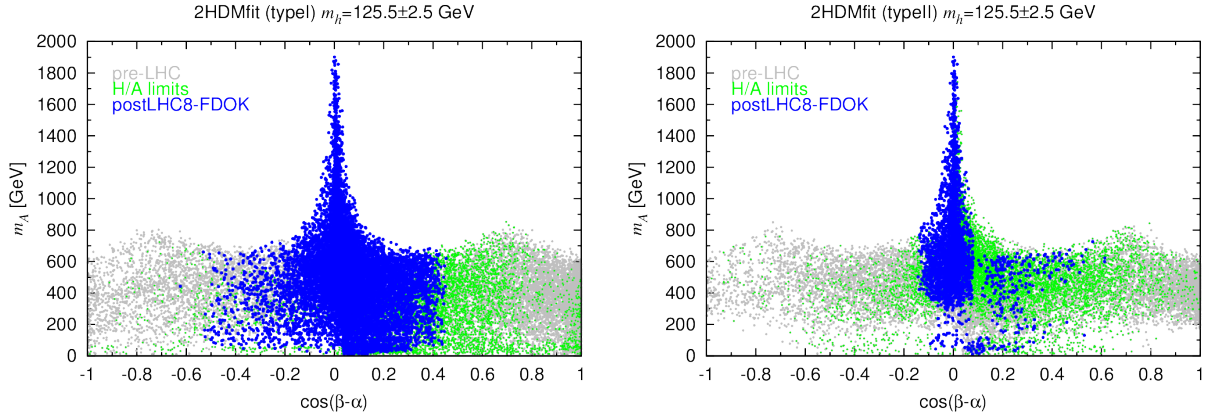

FIG. 4: Constraints in the m_A versus $\cos(\beta - \alpha)$ plane for $m_h \sim 125.5$ GeV. Color scheme as in Fig. 2. The corresponding results in the m_H vs. $\cos(\beta - \alpha)$ and $m_{H^\pm}$ vs. $\cos(\beta - \alpha)$ planes give essentially the same picture as for m_A, except that m_H and $m_{H^\pm}$ do not go below 125 GeV and 100 GeV (300 GeV) for Type I (Type II), respectively.

if the h is found to have very SM-like VV coupling, *i.e.* if $|\cos(\beta - \alpha)| \approx 0$, then m_A, m_H and $m_{H^\pm}$ could each take a large range of values. The larger $\cos(\beta - \alpha) > 0$ points in the Type II case are the same as the $C_D^h \sim -1$ points of Fig. 3. That they cannot occur at high m_H is associated with nondecoupling perturbativity limits, see [41].

To illuminate the precision with which individual channels are being fit, we show in Fig. 5 the signal strengths for $\mu_{gg}^h(ZZ)$ vs. $\mu_{gg}^h(\gamma\gamma)$ (upper row) as well as for $\mu_{\rm VBF}^h(\gamma\gamma)$ vs. $\mu_{gg}^h(\gamma\gamma)$

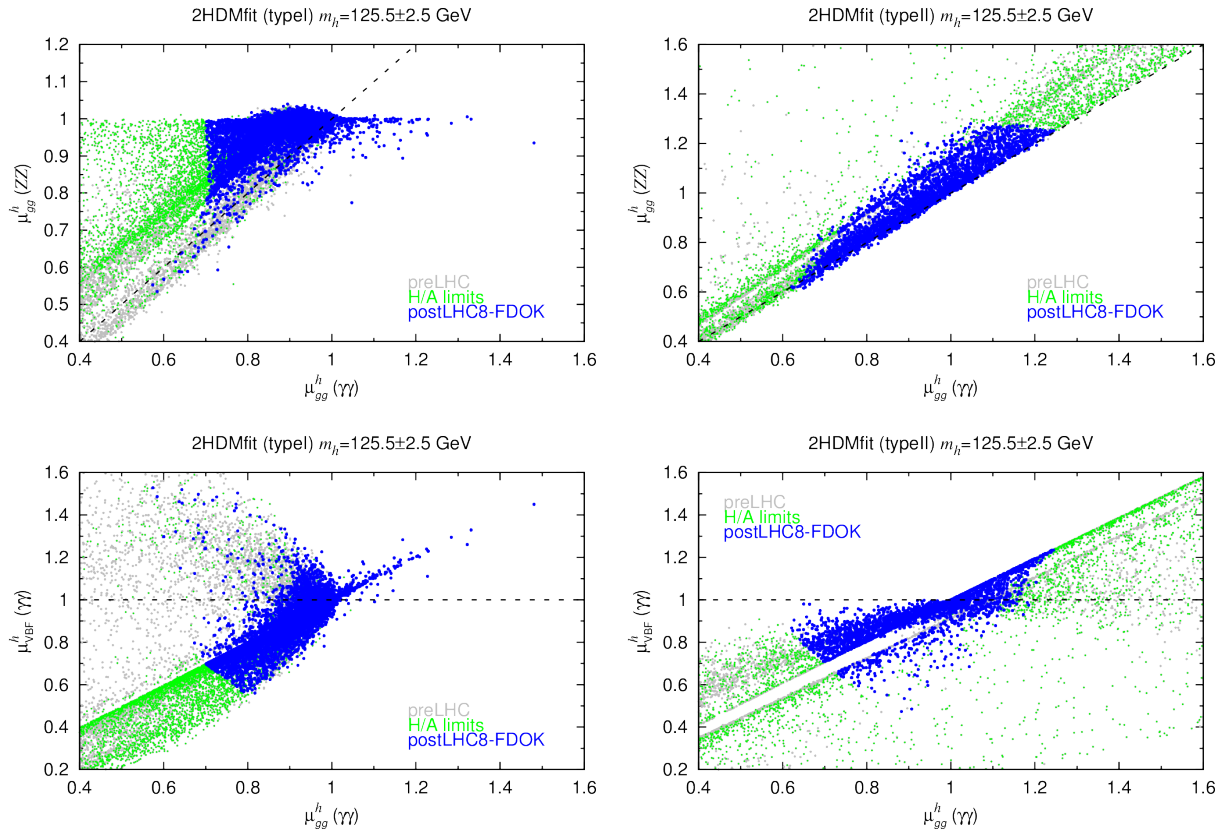

FIG. 5: Correlations of signal strengths for the $m_h \sim 125.5$ GeV scenario following the color scheme of Fig. 2; in the upper row $\mu^h_{gg}(ZZ)$ vs. $\mu^h_{gg}(\gamma\gamma)$, in the lower row $\mu^h_{\rm VBF}(\gamma\gamma)$ vs. $\mu^h_{gg}(\gamma\gamma)$.

(lower row). From this figure, it is apparent that requiring the μ values to lie within $\pm 10\%$ of unity would have a strong impact. Even $\pm 20\%$ measurements will remove many parameter choices. Note also that with sufficiently precise measurements of $\mu^h_{gg}(ZZ)$ and $\mu^h_{gg}(\gamma\gamma)$ there is a chance to distinguish Type I from Type II models; for most of the blue points if $\mu^h_{gg}(\gamma\gamma)$ is > 1, then $\mu^h_{gg}(ZZ)/\mu^h_{gg}(\gamma\gamma) < 1$ for Type I, whereas for Type II $\mu^h_{gg}(ZZ)/\mu^h_{gg}(\gamma\gamma) > 1$ always. Likewise, there are complementary correlations between the ggF and VBF modes, as illustrated for the $\gamma\gamma$ final state in the lower row of Fig. 5. In particular, if $\mu^h_{\rm VBF}(\gamma\gamma) > 1$, then $\mu^h_{gg}(\gamma\gamma) < 1$ is required in Type I, whereas just the opposite statement applies in Type II. In general, the cross correlations between different production$\times$decay modes carry interesting information because of the dependences in particular of the hgg and $h\gamma\gamma$ couplings on C_U, C_V (and in Type II for large $\tan\beta$ also on C_D) and thus can be useful for distinguishing scenarios.

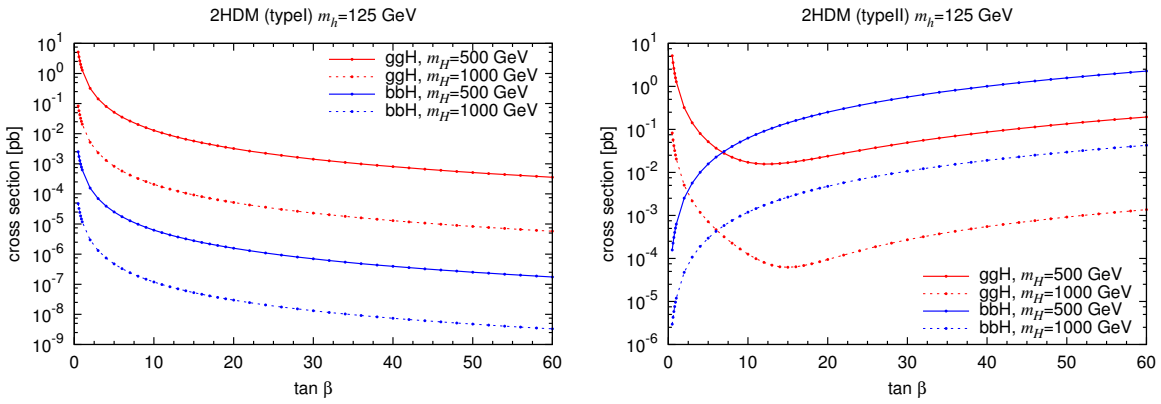

FIG. 6: Cross sections (in pb) for $gg \to H$ and bbH production at $\sqrt{s} = 8$ TeV as a function of $\tan\beta$ for $m_H = 500$ GeV and 1 TeV. The results shown are for the SM limit of $\sin(\beta - \alpha) = 1$.

With regard to the H/A limits coming from heavy Higgs bosons, we find that they have significant impact. In the case of Type I, the limits coming from $gg \to H, A \to \tau\tau$ are always stronger (even at high $\tan\beta$) than those coming from $gg \to b\bar{b}H, b\bar{b}A$ with $H, A \to \tau\tau$. This is because, in Type I models, all the fermionic couplings are the same and it is only a question of the $\tan\beta$-independent ratio of the $gg \to H, A$ cross section to the $gg \to b\bar{b}H, b\bar{b}A$ cross section. This ratio is always quite a bit larger than 1 (by typically a factor of at least 100) at any given mass. For Type II models, we note that the down-type coupling is enhanced by $\tan\beta$ and affects both production modes, in the $gg \to H, A$ case by enhancing the b-quark contribution to the one-loop coupling. To illustrate the comparison between these two production modes, we plot for two representative masses (500 GeV and 1 TeV) the two cross sections vs. $\tan\beta$ in Fig. 6 with α chosen so that $\sin(\beta - \alpha) = 1$. In the case of Type II, we observe that at low $\tan\beta$ it is $\sigma(gg \to H)$ that is biggest while at high $\tan\beta$ it is $\sigma(bbH)$ that is biggest by a factor of ~ 10 to 100.

B. Implications for the future

At this point, we turn to a consideration of what future measurements at LHC 13/14 or a linear collider might be most revealing. Let us first quantify the extent to which future higher precision measurements at the next LHC run might be able to restrict the model parameter space. Typical results are illustrated in Fig. 7. To make clear the impact of increased precision in the future, we will show points that survive if the observed values of

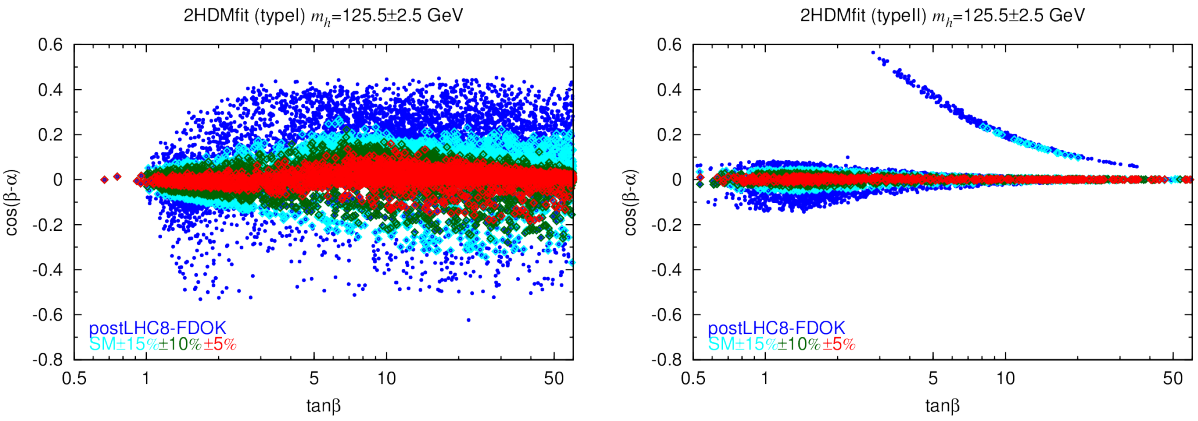

FIG. 7: The postLHC8-FDOK points in the $\cos(\beta-\alpha)$ vs. $\tan\beta$ plane for the $m_h \sim 125.5$ GeV scenario comparing current h fits (blue) to the case that the rates for all the channels listed in Eq. (6) are within ±15% (cyan), ±10% (green) or ±5% (red) of the SM Higgs prediction. FDOK is also required for these latter points.

$\mu_X^h(Y)$ *all* lie within P% of the SM prediction for the following channels (X,Y):[5]

$$(gg,\gamma\gamma),\ (gg,ZZ),\ (gg,\tau\tau),\ (\mathrm{VBF},\gamma\gamma),\ (\mathrm{VBF},ZZ),\ (\mathrm{VBF},\tau\tau)=(\mathrm{VH},bb),\ (\mathrm{ttH},bb)\,. \quad (6)$$

Here, we will consider $P = \pm15\%$, $\pm10\%$ and $\pm5\%$. For this we use the shorthand notation SM±15%, SM±10% and SM±5%, respectively. Not unexpectedly, as increasingly precise agreement with the SM is imposed in the various channels, one is quickly pushed to small $|\cos(\beta-\alpha)|$, but $\tan\beta$ remains unrestricted. Note that even SM±10% on each of the individual μ's will have eliminated the "wrong-sign" down-quark Yukawa region (which corresponds to $\sin\alpha > 0$ or $C_D^h < 0$) of the Type II model.

The reason for this is clarified by Fig. 8. Here, we require that the rates for the bb and $\tau\tau$ final states are consistent at 95% C.L. with current data and then examine the implications for $gg \to h \to \gamma\gamma$ when requiring that the $gg \to h \to ZZ$ and $VV \to h \to ZZ$ rates be progressively closer to the SM prediction. We see that once SM±10% is required for the ZZ final state, then $\mu_{gg}^h(\gamma\gamma)$ is at least 5% below the SM in the $\sin\alpha > 0$ region. As explained in [41] this is because for $\sin\alpha > 0$ the charged-Higgs loop contribution to the $h\gamma\gamma$ coupling

[5] It is important to note that the $(\mathrm{VBF},\tau\tau) = (\mathrm{VH},bb)$ channels have exactly the same scaling factor in 2HDMs. We mention them together since they are experimentally very different channels and although individually they may not be measurable with a certain level of accuracy, in combination they should be able to determine the common μ to the specified accuracy.

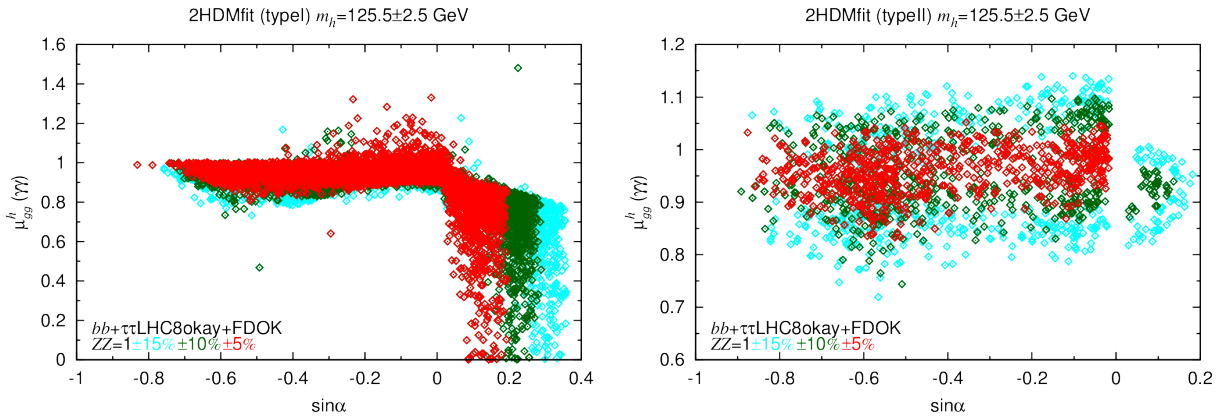

FIG. 8: The postLHC8-FDOK points in the $\mu^h_{gg}(\gamma\gamma)$ vs. $\sin\alpha$ plane for the $m_h \sim 125.5$ GeV scenario, requiring that the $gg \to ZZ$ and $VV \to ZZ$ rates are both within $\pm 15\%$ (cyan), $\pm 10\%$ (green) and $\pm 5\%$ (red) of the SM predictions. The individual rates for the $\tau\tau$ and bb final states are consistent with current 95% CL limits.

does not decouple and causes a decrease in $\Gamma(h \to \gamma\gamma)$ of order 10%. This decrease is only partially compensated by a 6% increase in the cross section for $gg \to h$ that arises due to the fact that the interference between the top and bottom loops has a sign that is opposite the normal sign in this $\sin\alpha > 0$ region. As regards the Type I model, the sign of the up-type and down-type Yukawa couplings is independent of the sign of $\sin\alpha$. Nonetheless, $\sin\alpha > 0$ values are disfavored since the $\mu^h_{gg}(\gamma\gamma)$ rate reduces as $\sin\alpha$ increases past zero. This is in fact also true in Type II models. As noted in relation to Fig. 1, this is a result of requiring that all quartic Higgs couplings remain perturbative, defined by having absolute values below 4π.

One quantity of particular interest for a SM-like h is the triple-Higgs coupling strength λ_{hhh}. We plot the current and possible future expectations in Fig. 9 for C_{hhh} (defined as the value of λ_{hhh} relative to the SM value). We observe that if the $\mu_X(Y)$ measurements were to have excursions from the SM predictions at the currently allowed 95% level extreme, then measurement of a large deviation from $C_{hhh} = 1$ would be quite likely (also see [42]). For example, at the high-luminosity LHC14, with $L = 3000$ fb^{-1} one can measure λ_{hhh} to the 50% level [43], and given the limited constraints on the model implied by current Higgs data, deviations from $C_{hhh} = 1$ of this order, indeed up to 100% or more, are possible. However, if future LHC measurements imply increasingly smaller deviations from $\mu_X(Y) = 1$ in the

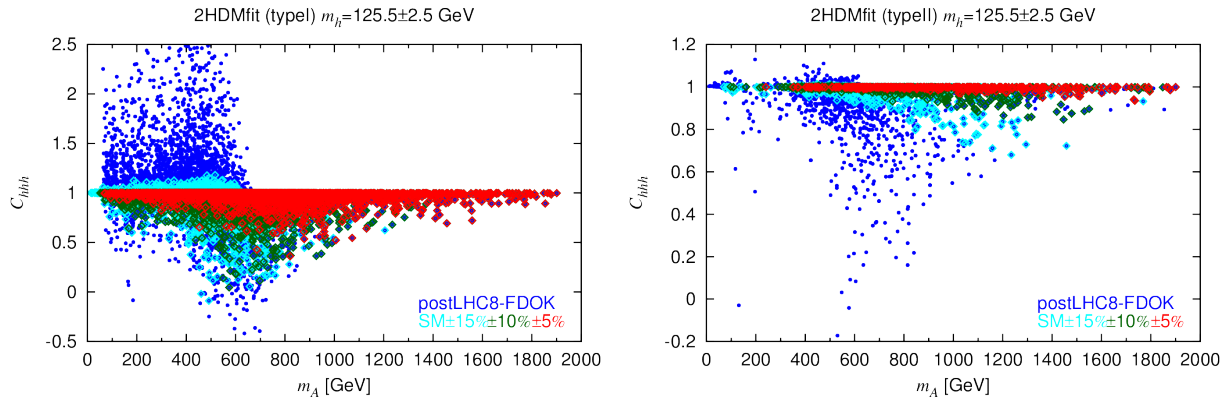

FIG. 9: The postLHC8-FDOK points in the C_{hhh} vs. m_A plane for the $m_h \sim 125.5$ GeV scenario comparing current h fits to the case where future measurements show that the rates for all the channels listed in Eq. (6) are within $\pm 15\%, \pm 10\%, \pm 5\%$ of the SM Higgs prediction; FDOK is required in all cases. Color scheme is as for Fig. 7.

various channels, then observing a deviation from $C_{hhh} = 1$ becomes increasingly difficult, even at the ILC. For example, from [43] we find that the predicted precision on λ_{hhh} for ILC1000 with $L = 500 - 1000$ fb^{-1} of 21% and for ILC1000 with $L = 1600 - 2500$ fb^{-1} is of order 13%. At CLIC3000 with $L = 2000$ fb^{-1} the accuracy achievable would be about 10%.

Comparing to the deviations shown in Fig. 9, we see that in Type I a determination of $\mu_X(Y)$ rates at the level of SM±10% still allows C_{hhh} as small as ~ 0, while SM±5% allows C_{hhh} as small as 0.3, either of which will be observable for any of the listed machines and integrated L values. In contrast, for Type II, even SM±15% would already imply that C_{hhh} must lie below 1. This agrees with the conclusion reached in [17] where it is stated that current 68% C.L. (1σ) limits (which are very close to our SM±15% constraint) imply $C_{hhh} \leq 1$ for Type II. We note further that the smallest C_{hhh} for SM±10% is ~ 0.9, while for SM±5% it is ~ 0.95. The former would require CLIC3000 while the latter would be beyond the reach of any of the above e^+e^- colliders. Thus, it is clear that future LHC Higgs data could have a very significant impact on the prospects for seeing an interesting deviation from $C_{hhh} = 1$ at ILC/CLIC. As an aside, we note from Fig. 9 that for Type II (but not Type I) models SM±5% is only possible for $m_A \gtrsim 250 - 300$ GeV depending on $\tan\beta$.

With this in mind, it is important to consider implications of the current and future h fits for the heavier Higgs bosons. Hopefully, one will retain a significant possibility of detecting

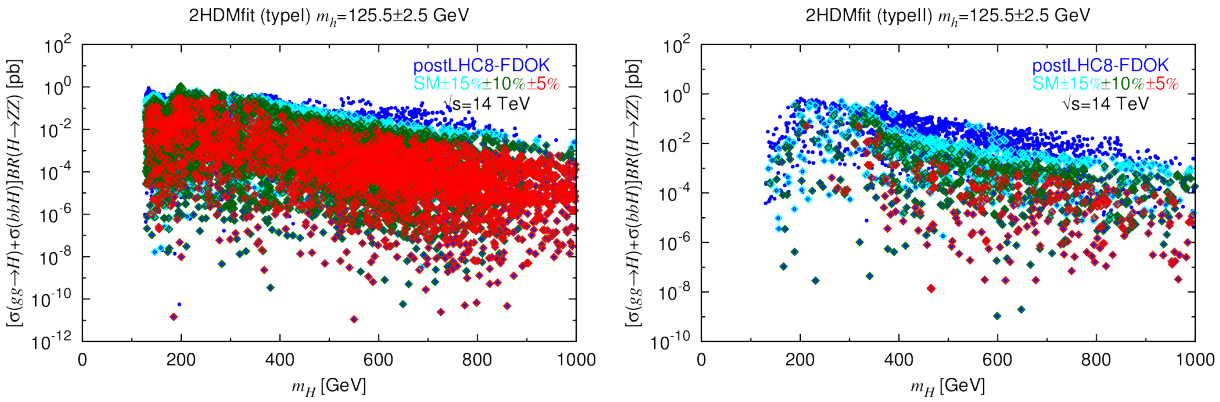

FIG. 10: We plot $[\sigma(gg \to H) + \sigma(bbH)]\mathrm{BR}(H \to ZZ)$ as functions of m_H, for Type I (left) and Type II (right) 2HDMs. Only FDOK points are shown. Implications of various levels of precision for future h measurements are displayed. Color scheme is as for Fig. 7.

the heavier Higgs bosons even if the h is shown to be very SM-like. To assess the situation, we consider only the high-rate gluon-fusion and bb associated production processes for the H and A.[6] There are many final states of potential interest. These include $H \to ZZ$, $H, A \to \tau\tau, \gamma\gamma, t\bar{t}$ as well as the $H \to hh$ and $A \to Zh$ final states.

Results for $H \to ZZ$ at $\sqrt{s} = 14$ TeV are shown in Fig. 10. We observe that substantial $\sigma \times \mathrm{BR}$ values (as high as ~ 1 pb at $m_H \sim 150$ GeV and ~ 1 fb at $m_H \sim 1$ TeV) are possible, but certainly not guaranteed. In the case of the Type II model, if the h is determined to have SM-like rates within $\pm 10\%$ or, especially, $\pm 5\%$ then the maximum possible $\sigma \times \mathrm{BR}$ is substantially reduced and the minimum allowed m_H for $\pm 5\%$ is of order 200 GeV.

Results for $gg + bb \to H, A$ production in the $\tau\tau$ final state are displayed in Fig. 11 assuming $\sqrt{s} = 14$ TeV. Overall, the range of possible cross sections is quite large, with maximum values of order 1 to 10 pb and minimum values below 10^{-10} pb in the case of Type I (although this range is somewhat narrowed on average as the h is required to be more and more SM-like) and minimum values of order $10^{-4} - 10^{-5}$ pb in the case of Type II. It is worth noting that for lower values of m_H and m_A, $[\sigma(gg \to H) + \sigma(bbH)]\mathrm{BR}(H \to \tau\tau)$ and $[\sigma(gg \to A) + \sigma(bbA)]\mathrm{BR}(A \to \tau\tau)$ are typically quite substantial in the Type II case,

[6] For reasons of space, we will mainly present results for the inclusively summed ggF and bb associated production of a given Higgs for $\sqrt{s} = 14$ TeV. Of course, it will be possible and of interest to separate these experimentally.

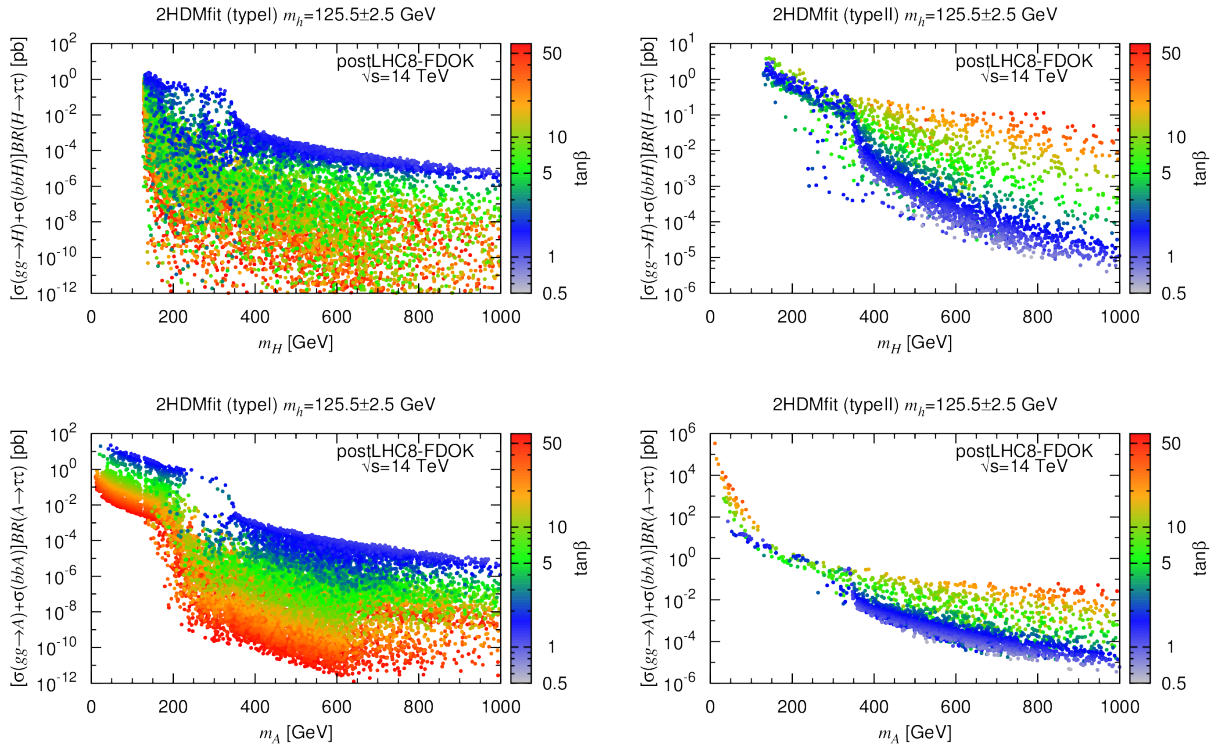

FIG. 11: Scatter plots of $[\sigma(gg \to H) + \sigma(bbH)]\mathrm{BR}(H \to \tau\tau)$ and $[\sigma(gg \to A) + \sigma(bbA)]\mathrm{BR}(A \to \tau\tau)$, in pb, as functions of m_H (top row) and m_A (bottom row), respectively, for postLHC8-FDOK points with $m_h \sim 125.5$ GeV. The values of $\tan\beta$ are color-coded as indicated on the plots.

but that few points survive below $m_H \sim 300$ GeV if the 125.5 GeV state rates lie within 5% of the SM Higgs predictions. We comment on one particular feature of the plots, namely the fact that the $t\bar{t}$ threshold is not apparent for Type II in the case of the A. This is a direct consequence of the fact that the LHC8 constraints include the limits from [35] on $gg \to A$ and bbA with $A \to \tau\tau$. The predicted 2HDM cross sections can significantly exceed these limits in the region below $2m_t$. Since these limits are included in obtaining the postLHC8 results the $t\bar{t}$ threshold that would otherwise be apparent is not present. Note that in the case of the H, the limits of [35] do not have a strong impact because the predicted values of $\sigma(gg \to H)\mathrm{BR}(H \to \tau\tau)$ are smaller due to the fact that $H \to ZZ$ decays are also present.

It is also interesting to consider the $\tan\beta$ dependence of the cross sections, indicated by a color code in Fig. 11. As expected from the fermionic couplings in Table I, this dependence is opposite in Type I and Type II. Concretely, in Type I $[\sigma(gg \to H) + \sigma(bbH)]\mathrm{BR}(H \to \tau\tau)$ and $[\sigma(gg \to A) + \sigma(bbA)]\mathrm{BR}(A \to \tau\tau)$ increase as $\tan\beta$ gets smaller, while in Type II larger

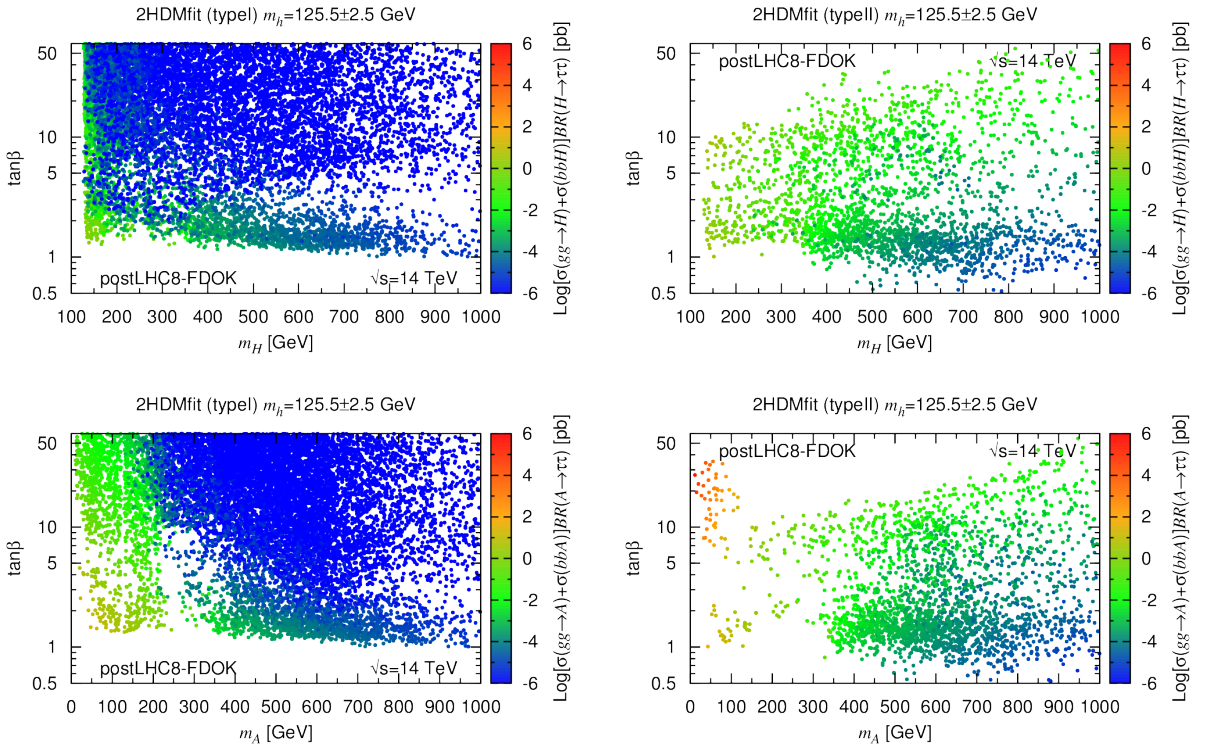

FIG. 12: Same information as in Fig. 11 but in the $\tan\beta$ vs. m_H (top row) and $\tan\beta$ vs. m_A (bottom row) planes with the 14 TeV cross sections color coded as indicated by the scales on the right of the plots. Only FDOK points are shown.

cross sections are obtained for larger $\tan\beta$. Note also that in Type II the $t\bar{t}$ threshold is visible for small $\tan\beta \lesssim 3$ but not for larger values.

In the case of the Minimal Supersymmetric Standard Model (MSSM), which is a special case of a Type II model, limits on $H, A \to \tau\tau$ are often presented in the $\tan\beta$ vs. m_A plane. For the sake of comparison, we show in Fig. 12 the $H, A \to \tau\tau$ rates (in pb) in the $\tan\beta$ vs. m_H (top row) and $\tan\beta$ vs. m_A (bottom row) planes for both Type I and Type II, plotting, however, only points with $\sigma > 10^{-6}$ pb. We note a very interesting difference with the MSSM case. In the 2HDMs, it is possible to have small m_A independent of the other Higgs masses. Further, small m_A can escape LEP limits provided, in particular, that hA production is sufficiently suppressed. This is natural in the present case to the extent that $\sin(\beta-\alpha) \sim 1$ for a SM-like h given that the ZAh coupling is $\propto \cos(\beta-\alpha)$. This is the origin of the points in the bottom right plots of Figs. 11 and 12 with $m_A \lesssim 100$ GeV and a very large cross section. (Note that CMS and ATLAS 8 TeV constraints on the $\tan\beta$ vs. m_A

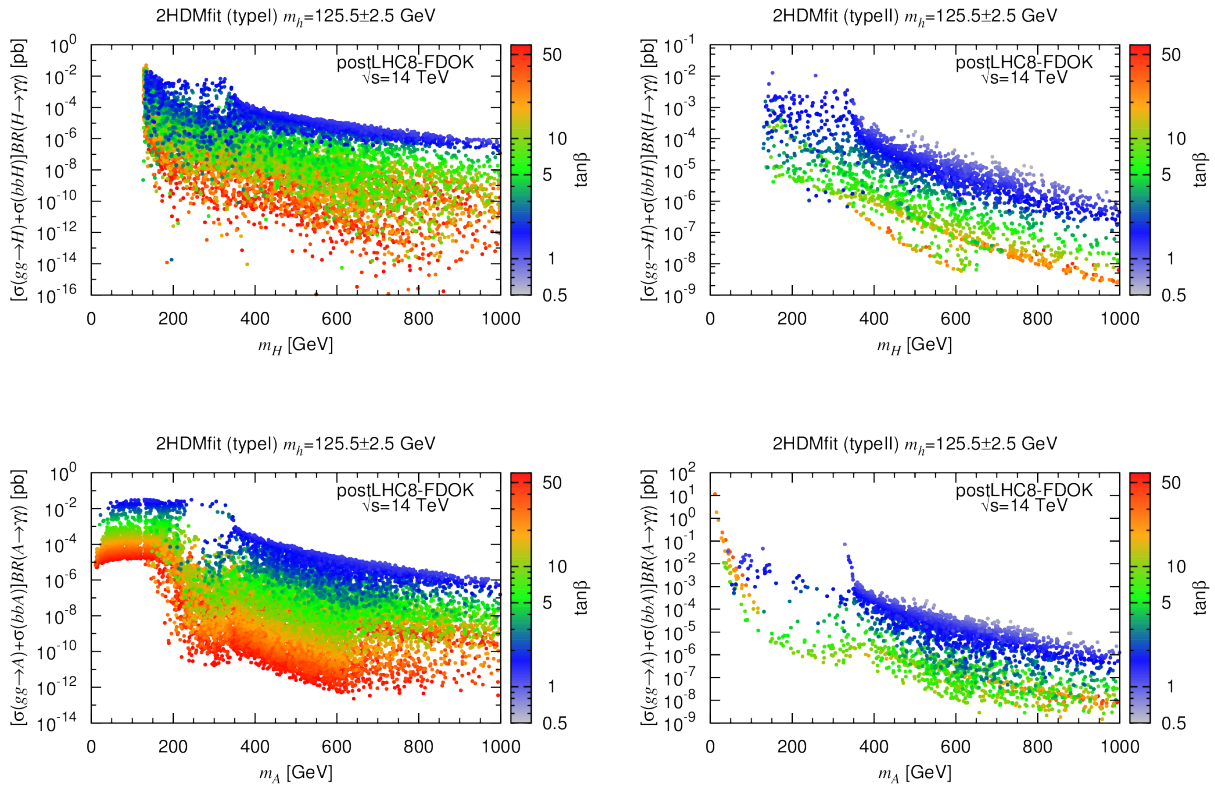

FIG. 13: Scatterplots of $[\sigma(gg \to H) + \sigma(bbH)]\mathrm{BR}(H \to \gamma\gamma)$ as function of m_H (top row) and $[\sigma(gg \to A) + \sigma(bbA)]\mathrm{BR}(A \to \gamma\gamma)$ as function of m_A (bottom row), for postLHC8-FDOK points with $m_h \sim 125.5$ GeV. The values of $\tan\beta$ are color coded as indicated by the scales on the right of the plots.

plane (not shown) do not exist below ~ 90 GeV. Furthermore, we have explicitly checked that these limits do allow the few points shown with $m_A \gtrsim 90$ GeV.)

As an aside, we note that in both the H and A cases the $\mu\mu$ final state rates are obtained by simply multiplying by the relevant ratio of branching ratios, $\mathrm{BR}(H \text{ or } A \to \mu\mu)/\mathrm{BR}(H \text{ or } A \to \tau\tau)$, which is essentially independent of $\tan\beta$ in either Type I or Type II with a value of order 3.5×10^{-3}. Looking at Fig. 11, it would appear that prospects for detecting the H and A in the $\mu\mu$ final state are significant for m_A and m_H below the top threshold, especially in the case of $A \to \mu\mu$ in Type II when $m_A \lesssim 150$ GeV.

Corresponding results for the $H \to \gamma\gamma$ and $A \to \gamma\gamma$ final states are shown in Fig. 13. Aside from $m_A \lesssim 50$ GeV in Type II, the largest $\sigma \times \mathrm{BR}$'s are of order 0.05 pb, with much

lower values being more typical. If the $\gamma\gamma$ continuum background is sufficiently small, $\sigma \times$BR values as low as $10^{-3} - 10^{-4}$ pb might well be observable, although it must be kept in mind that the total width of the H or A will be of order several to a few tens of GeV.

In the preceding plots, we have not displayed the impact of future h measurements that lie within SM±15%, SM±10% and SM±5%. In the case of Type I, agreement with the SM of ±10% or better implies that $m_A \lesssim 80$ GeV is excluded (whereas at the postLHC8 level very low m_A is allowed). This is apparent from examining the reach in m_A in Fig. 9. In the case of m_H, which already must lie above ~ 125.5 GeV, there is almost no impact as increasing agreement with the SM is required. For Type II, the impact is more varied. In the case of the A, as one moves through SM±15%, 10%, 5% fewer and fewer points are found at lower m_A, as can again be read from Fig. 9, but determining precise boundaries would require dedicated scanning. In the case of the H, SM±15% and ±10% do not restrict m_H beyond the postLHC8 range, but heavier m_H is preferred by SM±5%.

Of course, once m_A or m_H is above the $t\bar{t}$ threshold, the rates in the $t\bar{t}$ final state will be of great interest. These are shown in Fig. 14. Large $\sigma \times$ BR values are certainly possible, but so also are very small values, although in the case of Type II the smallest values found at m_H or m_A of order 1 TeV is $\sim 10^{-4}$ pb. This latter might be detectable for full Run2 luminosity of $L = 300$ fb^{-1}, and is certainly of great interest for the high-luminosity run of the LHC which might accumulate $L = 3000$ fb^{-1}.

Perhaps most interesting are the rates for $H \to hh$ and $A \to Zh$. First, we show in Fig. 15 the results for ggF at $\sqrt{s} = 8$ TeV. These results should be compared to the ggF limits obtained recently in [32], which are shown as black lines in the plots of Fig. 15; see also projections at the 14 TeV LHC in [44]. Moreover, we show the points that have significant FD (as discussed in detail in the following subsection). We distinguish between points for which the amount of FD violates the FDOK criteria, but is still moderate in size (orange points, labelled "Low FD"), as defined below in Section III C, and points with a high level of FD (red points, labelled "High FD"). In the case of $H \to hh$, none of the points are excluded by [32], not even the High FD ones. In the case of $\sigma(gg \to A)\text{BR}(A \to Zh)$, on the other hand, the experimental limits exclude a significant fraction of the High FD points in the case of Type I models. In the case of Type II, only a few of the High FD points are excluded. Nonetheless, the nearness of the black line limits to the High FD points indicates

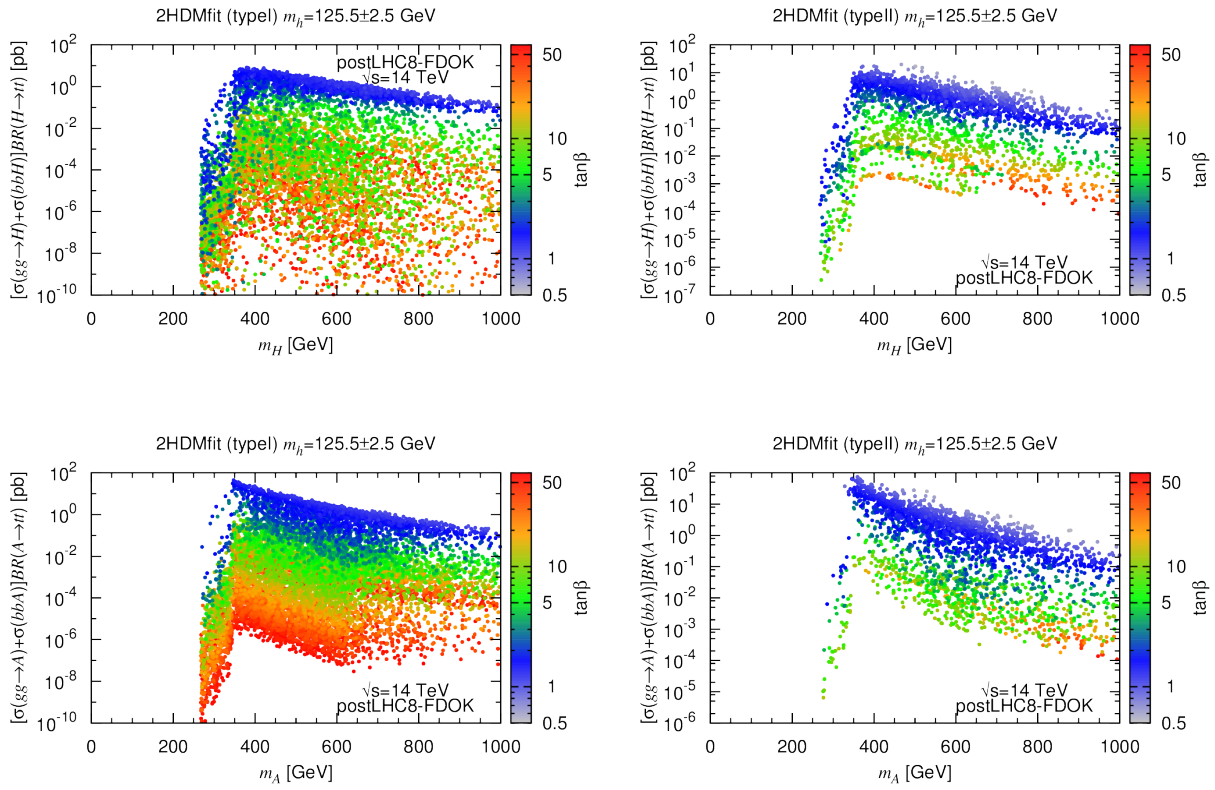

FIG. 14: Scatter plots of $[\sigma(gg \to H) + \sigma(bbH)]\text{BR}(H \to t\bar{t})$ as function of m_H (top row) and $[\sigma(gg \to A) + \sigma(bbA)]\text{BR}(A \to t\bar{t})$ as function of m_A (bottom row) at $\sqrt{s} = 14$ TeV, for postLHC8-FDOK points with $m_h \sim 125.5$ GeV. The values of $\tan\beta$ are color coded as indicated by the scales on the right of the plots.

that we should not be surprised if the above two processes are the dominant sources of feed down, as we shall describe in the next section.

From Fig. 15 we see that the points with unacceptable FD levels are prominent in the $m_H \sim 250-350$ GeV region and, especially, in the $m_A \sim 200-350$ GeV region. Looking back at, for example, Figs. 11 and 13, which include only postLHC8-FDOK points, we observe corresponding "holes" and depleted regions at low $\tan\beta$ in precisely these mass regions. FD is largest at low $\tan\beta$ where $\sigma(gg \to A, H) + \sigma(bbA, bbH)$ is largest, as is especially true in the case of Type I models. In these figures, the surviving points that surround or outline the depleted regions are ones with very small $\cos(\beta - \alpha)$ which implies very small AZh coupling and therefore very small $\text{BR}(A \to Zh)$ ($A \to Zh$ being the feed down mechanism of primary

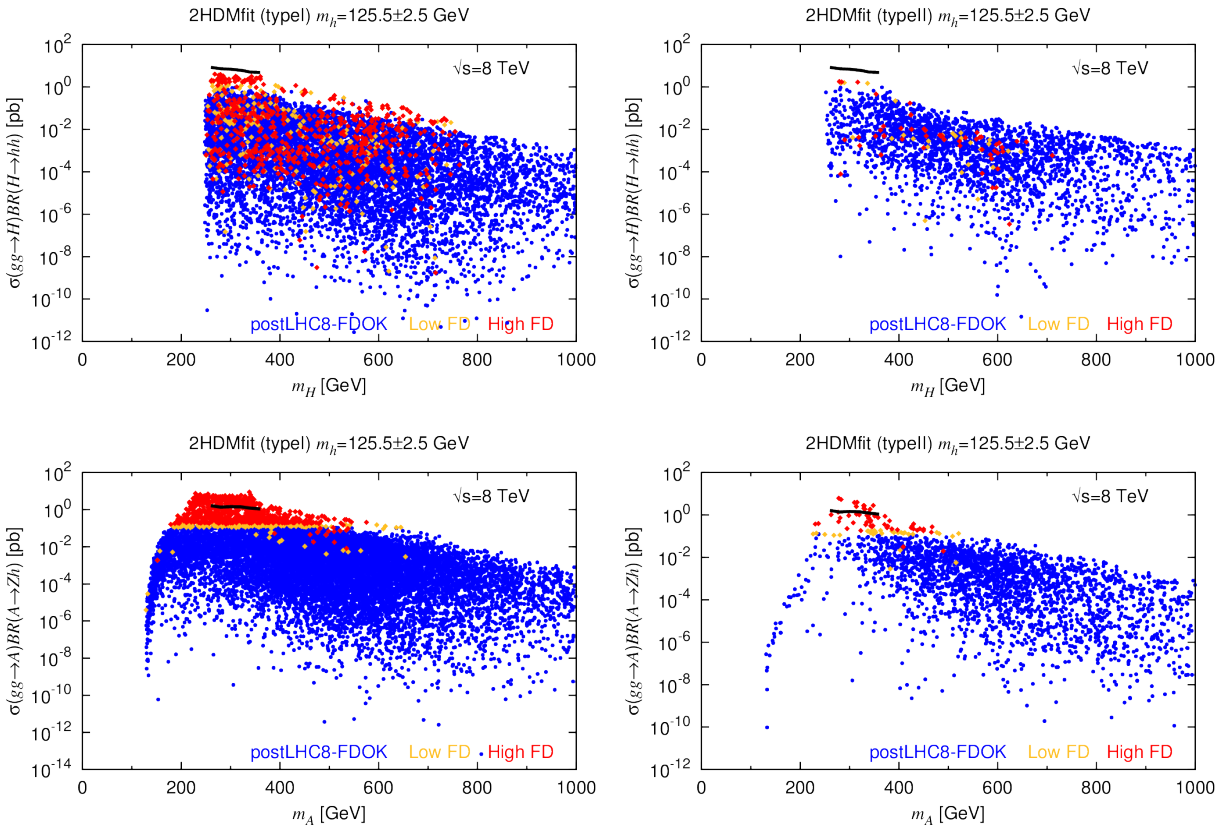

FIG. 15: We plot $\sigma(gg \to H)\mathrm{BR}(H \to hh)$ and $\sigma(gg \to A)\mathrm{BR}(A \to Zh)$ as functions of m_H and m_A, respectively, for Type I (left) and Type II (right) 2HDMs. Blue points fulfill all constraints, including the FDOK requirement. Also shown are the points that have Low FD (in orange) and High FD (in red) as defined in Section III C. The black lines show the current limits from the CMS analysis of Ref. [32].

importance, see Section III C).

It is interesting to note that to the extent that the $gg \to A \to Zh$ process contaminates direct Zh production whereas feed down to the Wh final state is substantially smaller (see later discussion), one might observe an apparent violation of custodial symmetry when extracting the C_Z and C_W effective coupling strengths independently of one another using Zh and Wh production, respectively. The fact that the direct limits in Fig. 15 are above the points that have large feed down indicates that apparent custodial symmetry violation might actually be a more sensitive probe of the presence of $H \to hh$ and, especially, $A \to Zh$ decays.

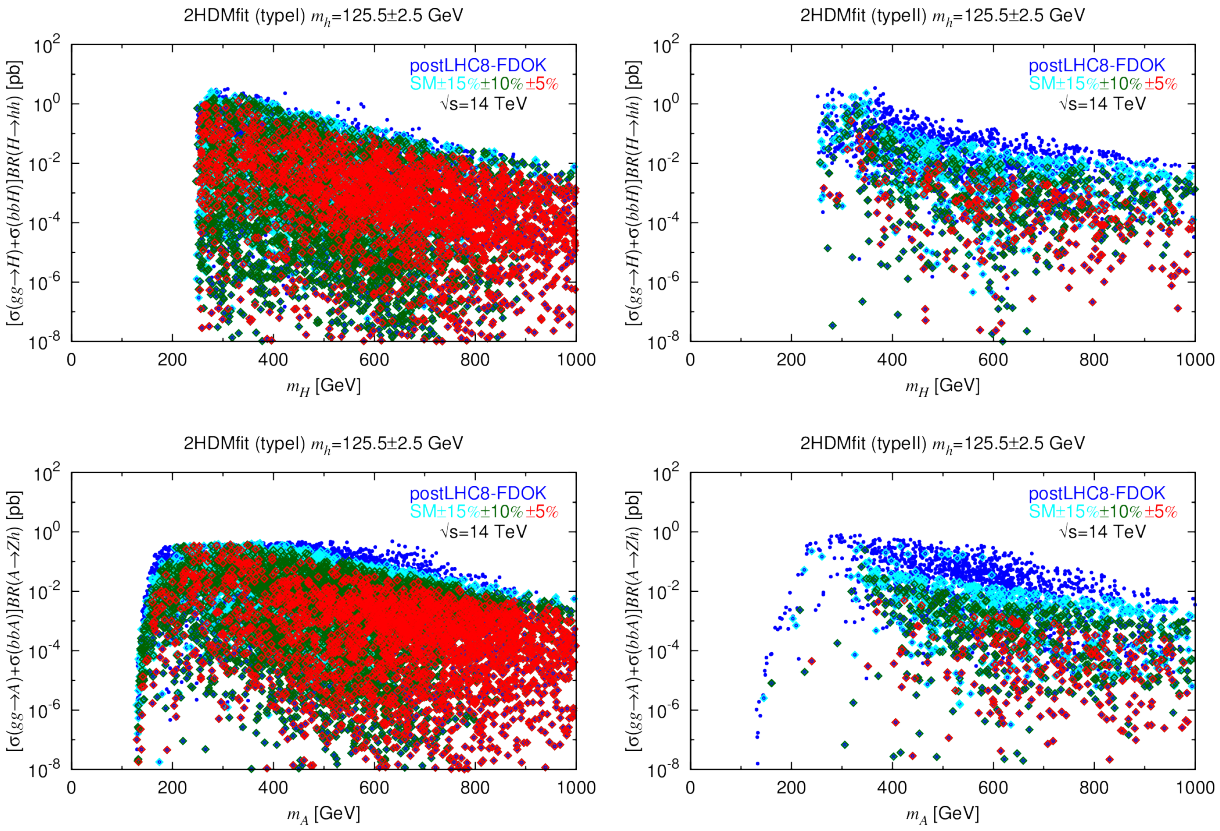

FIG. 16: We plot $[\sigma(gg \to H) + \sigma(bbH)]\mathrm{BR}(H \to hh)$ and $[\sigma(gg \to A) + \sigma(bbA)]\mathrm{BR}(A \to Zh)$ as functions of m_H and m_A, respectively, for Type I (left) and Type II (right) 2HDMs. For this figure, only FDOK points are shown. Implications of various levels of precision for future h measurements are displayed. Color scheme as in Fig. 7. Values of $\sigma \times$ BR below 10^{-8} are not plotted.

In Fig. 16 we show results for the hh and Zh final states for $\sqrt{s} = 14$ TeV, this time indicating the impact of SM±15%, ±10%, ±5% requirements. We note that if the h measurements approach SM values, then this will limit only somewhat the maximum values achievable for the cross section in the hh and Zh final states in the case of Type I models — which means that there is a significant, although not large, probability of seeing the $H \to hh$ and $A \to Zh$ final states in gluon fusion and in associated production with b quarks. However, in the case of Type II models, increasingly SM-like h results imply much smaller cross sections than those shown (as allowed by current Higgs fitting for both hh and Zh final states).

C. Feed down of heavier Higgs to the 125.5 GeV h

Let us now turn to the issue of whether feed down from heavier Higgs decaying to the ~ 125.5 GeV Higgs could invalidate our fitting. All the blue points plotted earlier are such that FD is neglectable in all channels of interest. The reason to be concerned is that heavy Higgs bosons have a propensity for decaying to a vector boson plus a Higgs boson or to two Higgs bosons. The most direct cases are $H \to hh$ and $A \to Zh$, but there are also chains like $H \to AA$ followed by $A \to Zh$ or $H \to H^+H^-$ with $H^\pm \to W^\pm h$ and so forth. The full formalism for the feed down calculations is given in Appendix A. For the present purposes, we will consider the most important FD sources and associated ratios

$$\mu^{\rm FD}_{{\rm ggF}h+{\rm bb}h} \equiv \frac{\sum_{\mathcal{H}=H,A}\left(\sigma_{{\rm ggF}\mathcal{H}}+\sigma_{bb\mathcal{H}}\right)P_{\rm FD}(\mathcal{H}\to h+X)}{\sigma_{{\rm ggF}h}+\sigma_{bbh}}\,, \tag{7}$$

$$\mu^{\rm FD}_{Zh} \equiv \frac{\sigma_{{\rm ggF}A}{\rm BR}(A\to Zh)}{\sigma_{Zh}}\,, \tag{8}$$

where $P_{\rm FD}(\mathcal{H}\to h+X)$ is the net branching ratio to produce one (or more) h in the $\mathcal{H}=H$ or A decay chains — see Appendix A. Above, $\sigma_{{\rm ggF}\mathcal{H}}$ and $\sigma_{bb\mathcal{H}}$ refer to the cross sections for $gg\to\mathcal{H}$ and $bb\mathcal{H}$ associated production respectively, where $\mathcal{H}$ can in the present case be H or A.

We emphasize that the amount of FD is computed without accounting for any reduced efficiency for accepting such events into the 125.5 GeV signal as a result of the experimental cuts used to define the $gg\to h$, bbh or $Z^*\to Zh$ channels. In practice, it could be that the actual FD after the experimental cuts currently employed to define the various channels is considerably smaller than this maximally conservative estimate.

In Fig. 17, we exhibit a few features of $\mu^{\rm FD}_{Zh}$ and $\mu^{\rm FD}_{{\rm ggF}h+{\rm bb}h}$. The upper two plots show the relative importance of $\mu^{\rm FD}_{Zh}$ compared to $\mu^{\rm FD}_{{\rm ggF}h+{\rm bb}h}$. We observe that the FD to the Zh final state from $A\to Zh$, $\mu^{\rm FD}_{Zh}$, is almost always the largest due to the large $gg\to A$ production rate compared to the $Z^*\to Zh$ rate that defines the $\mu^h_{V{\rm H}}(Zh)$ ratio that is the fundamental LHC measurement of interest.

We must now ask what amount of feed down is too large in the ggFh+bb$h$ and the Zh cases. This, of course, depends upon the accuracy with which the ggFh+bb$h$ and Zh channels are measured. At LHC8, very roughly, ggFh+bb$h$ and Zh channels are measured to accuracies of order 15% and of order 50%, respectively. Thus, we adopt the following criteria:

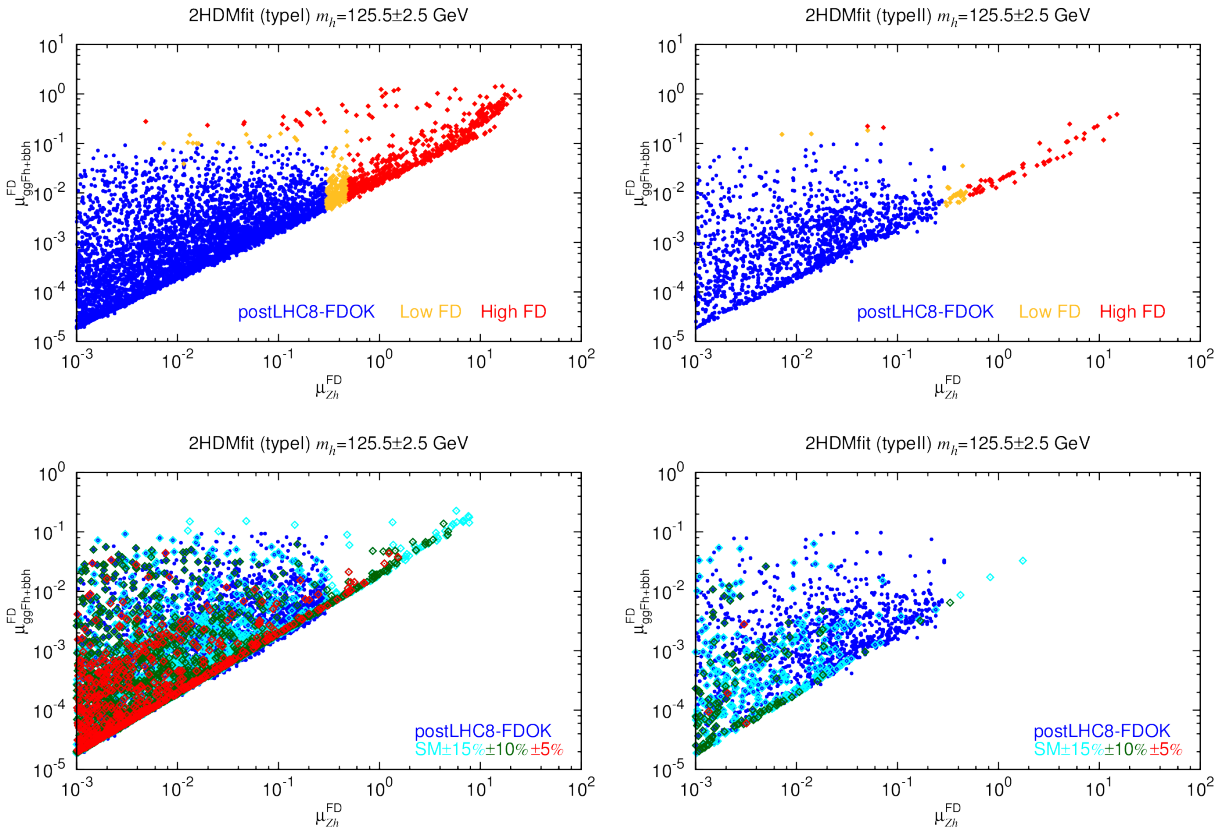

FIG. 17: Scatterplots of $\mu^{\rm FD}_{{\rm ggF}h+{\rm bb}h}$ vs. $\mu^{\rm FD}_{Zh}$. Top plots illustrate how high the FD fractions can go for postLHC8 points (not imposing any FD limit). The plots in the lower row illustrate how convergence of the h properties to SM-like values would limit the maximum possible FDs. We display only points with $\mu^{\rm FD}_{Zh} \geq 10^{-3}$ — there are many points with much lower values.

- In order for FD not to affect our fits we should have $\mu^{\rm FD}_{{\rm ggF}h+{\rm bb}h} \leq 0.1$ and $\mu^{\rm FD}_{Zh} \leq 0.3$. Points satisfying both criteria were already denoted as "FDOK" above.

- We further define "Low FD" as being cases such that FDOK criteria are violated by virtue of $0.1 < \mu^{\rm FD}_{{\rm ggF}h+{\rm bb}h} \leq 0.2$ and/or $0.3 < \mu^{\rm FD}_{Zh} \leq 0.5$.

- Finally, "High FD" is defined as $\mu^{\rm FD}_{{\rm ggF}h+{\rm bb}h} > 0.2$ and/or $\mu^{\rm FD}_{Zh} > 0.5$.

The lower two plots of Fig. 17 illustrate the fact that as the 125.5 GeV resonance is shown to be closer and closer to SM-like in all the various channels the maximum amount of FD that is possible is greatly reduced, becoming quite small for the SM±5% case. Increased precision in the signal strength measurements thus reduces the "danger" of FD contamination.

To illustrate the effect of FD, we repeat the plots of Figs. 2 and 4 in Fig. 18 showing additional points that have Low FD or High FD in at least one of the channels discussed above. In these plots, the orange (red) points are those for which we have Low FD (High FD). Note that the points in the plots of Fig. 18 with Low FD or High FD all correspond to moderate $\tan\beta$ (up to ~ 10). However, these points overlap those having an acceptable FD level. Thus, imposing the FD limits does not actually constrain the parameter spaces of the Type I or Type II models.

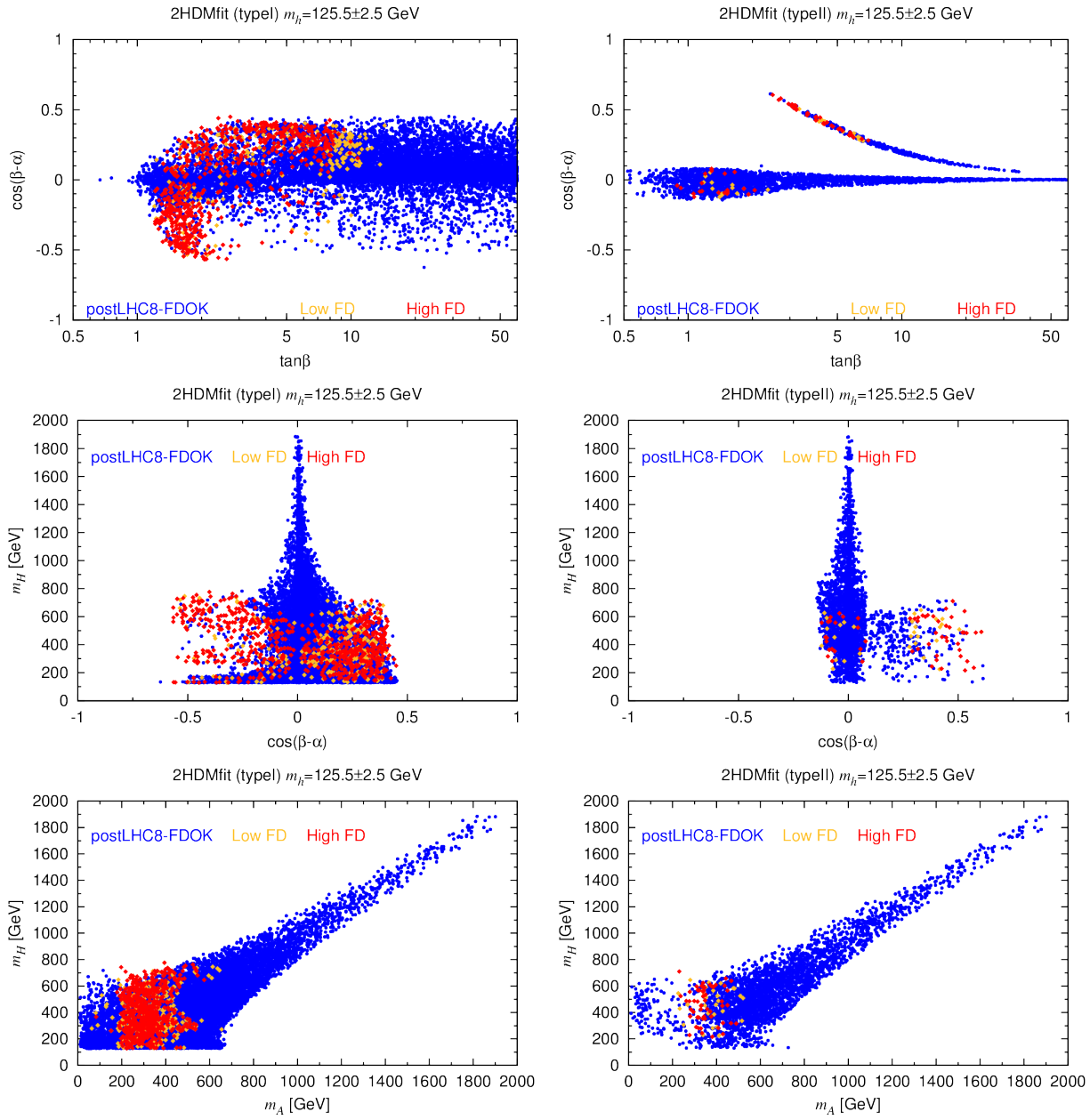

FIG. 18: Constraints in the planes $\cos(\beta-\alpha)$ vs. $\tan\beta$ (top row), m_H vs. $\cos(\beta-\alpha)$ (middle row) and m_H vs. m_A (bottom row) for $m_h \sim 125.5$ GeV. The blue points are the postLHC8-FDOK points. The orange (red) points are allowed postLHC8, but have Low FD (High FD). Many, but not all, Low FD and High FD points have postLHC8-FDOK points hidden below. Regarding the m_H vs. $\cos(\beta-\alpha)$ plots, replacing m_H by m_A or $m_{H^\pm}$ gives essentially the same picture.

IV. $m_H \sim 125.5$ GeV SCENARIOS

Let us now turn to the case that the observed SM-like Higgs near 125.5 GeV is the heavier CP-even state of the 2HDM, H. In this case, the lighter state, h, must have escaped LEP searches. However, we will see that a signal for the h could be hiding in the present data from the LHC and might be revealed in several focused analyses. The pseudoscalar A can be either lighter or heavier than the H. Since perturbativity for the quartic couplings prevents the A from being heavier than about 1 TeV, it can also give interesting signatures at LHC14.

We begin by presenting in Fig. 19 plots for the $m_H \sim 125.5$ GeV scenarios analogous to those of Fig. 2 for the $m_h \sim 125.5$ GeV scenarios. Here, we have again required small FD (from A production and decays); possible FD contributions will be discussed later in this section. In the case of Type I, consistency with the observed 125.5 GeV signal restricts $\sin(\beta-\alpha)$ less than was the case for $\cos(\beta-\alpha)$ in the $m_h \sim 125.5$ GeV case. In contrast, for Type II the constraints on $\sin(\beta-\alpha)$ are similar in nature to the limits on $\cos(\beta-\alpha)$ in the case of the h. There is, however, an important difference. Namely, if $\pm 5\%$ agreement with the SM can be verified in all the channels listed in Eq. (6), then $m_H = 125.5$ GeV is eliminated in Type II but not in Type I. This can be traced to the fact that the charged-

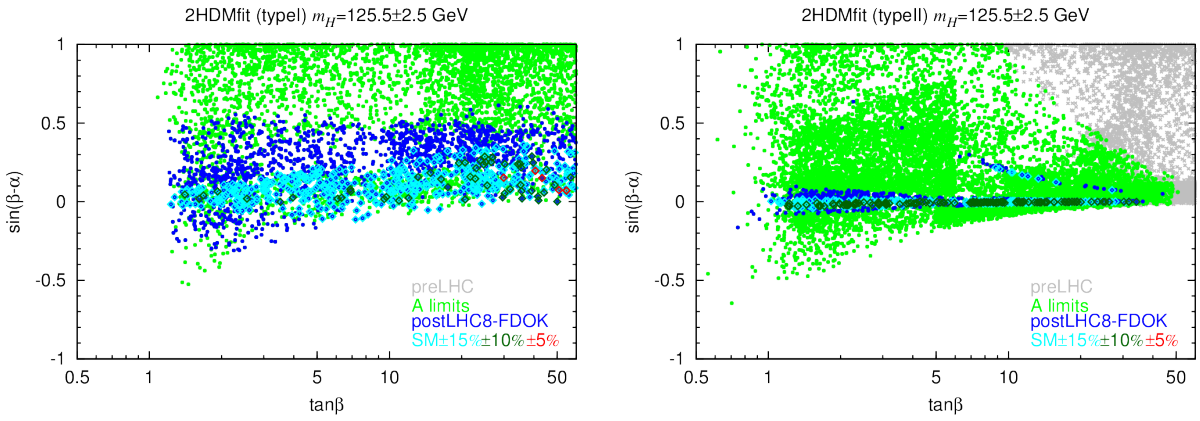

FIG. 19: Constraints on the 2HDM of Type I and Type II in the $\sin(\beta-\alpha)$ versus $\tan\beta$ plane for $m_H \sim 125.5$ GeV. We show points that survive at the preLHC (grey), A-limits (green), postLHC8-FDOK (blue), SM±15% (cyan), SM±10% (dark green), and SM±5% (red) levels. There are no FDOK requirements imposed on the preLHC and A-limits points. The SM$\pm 15\%, \pm 10\%, \pm 5\%$ points *are* subjected to FDOK requirements.

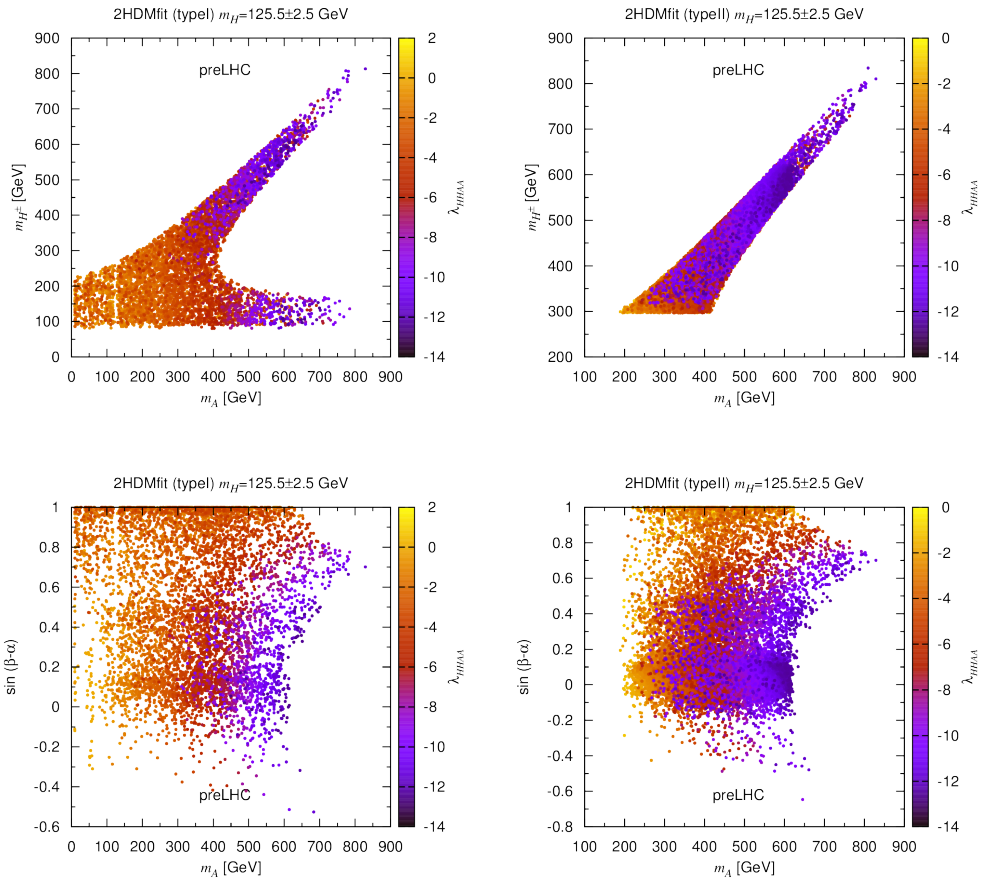

FIG. 20: Scatterplots of λ_{HHAA} in the $m_{H^\pm}$ vs. m_A and m_A vs. $\sin(\beta-\alpha)$ planes for the case of $m_H \sim 125.5$ GeV. The values of λ_{HHAA} are color coded as indicated by the scales on the right of the plots. The full set of preLHC conditions is satisfied for all points shown.

Higgs loop does not decouple at large $m_{H^\pm}$ and ends up suppressing the $H\gamma\gamma$ coupling and therefore the $\gamma\gamma$ final state rates. More details regarding the nondecoupling of the charged Higgs loop contribution to the $H\gamma\gamma$ coupling are presented in Appendix B.

There is a maximum $m_{H^\pm}$ that can be achieved before perturbativity is violated, but this maximum applies for all parameter choices, unlike the $m_h = 125.5$ GeV case for which there is a true decoupling limit. To illustrate this, we present in Fig. 20 (upper row) "temperature" plots showing the quartic coupling λ_{HHAA} in the plane of $m_{H^\pm}$ vs. m_A. λ_{HHAA} is one of a few that most frequently encounter the perturbativity bound. We see that λ_{HHAA} hits its perturbativity bound of $\sim 4\pi$ at about $m_A \sim m_{H^\pm} \sim 800$ GeV for both Type I and Type II. In the Type I case the perturbativity limit is also reached at low $m_{H^\pm}$ if m_A is as heavy as

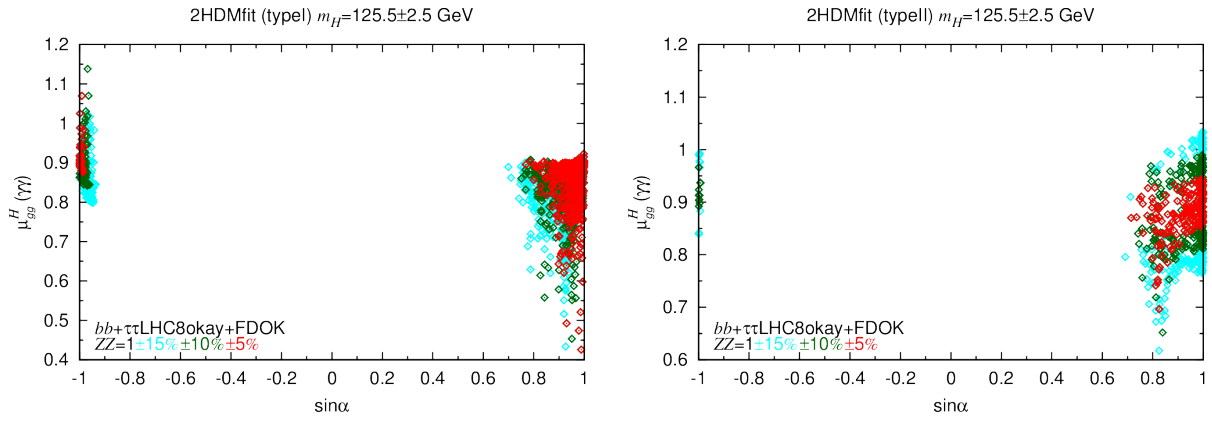

FIG. 21: We plot $\mu^H_{gg}(\gamma\gamma)$ as a function of $\sin\alpha$ for points having $gg \to ZZ$ and $VV \to ZZ$ rates within $\pm 15\%$, $\pm 10\%$ or $\pm 5\%$ of the SM predictions.

~ 800 GeV. This wing of the $m_{H^\pm}$ vs. m_A plot is not present for Type II because of the lower bound of about 300 GeV from B physics constraints. In the bottom row of Fig. 20 we present temperature plots of λ_{HHAA} in the m_A vs. $\sin(\beta-\alpha)$ plane, showing that at small to moderate $|\sin(\beta-\alpha)|$ the perturbative bound is already exceeded by $m_A \sim 600$ GeV. In any case, the bottom line is that there is no decoupling limit for the $m_H = 125.5$ GeV case and nondecoupling effects are inevitably of importance.

The resulting $\gamma\gamma$ final state rates are illustrated in Fig. 21. There, we see that consistency with $\pm 5\%$ for the ZZ final state rates and *simultaneously* for the $gg \to H \to \gamma\gamma$ rate is only possible on the $\sin\alpha < 0$ (*i.e.* $C^H_U < 0$) branch in the Type I model. Most of this mismatch can, as said earlier, be traced to the nondecoupling of the charged-Higgs loop contribution to the $H\gamma\gamma$ coupling. In the end only the few red points on the $\sin\alpha < 0$ branch of the Type I model having $\mu^H_{gg}(\gamma\gamma) \gtrsim 0.95$ can survive if $\leq \pm 5\%$ deviations from the SM are required for both the ZZ and $\gamma\gamma$ final states.

As regards the h and A masses associated with a good fit by the H to the LHC data and other limits we refer to Fig. 22. There, we see that a proper fit at the postLHC8 level is easily achieved if $m_h \gtrsim 60$ GeV, for which $H \to hh$ decays are kinematically forbidden. However, there is also a scattering of points for which small values of m_h are possible. Such points correspond to parameters for which the Hhh coupling is small. A very "fine-tuned" scan is necessary to find these low-m_h points for which BR$(H \to hh)$ is small enough that the H signals fit the LHC data at an adequate level.

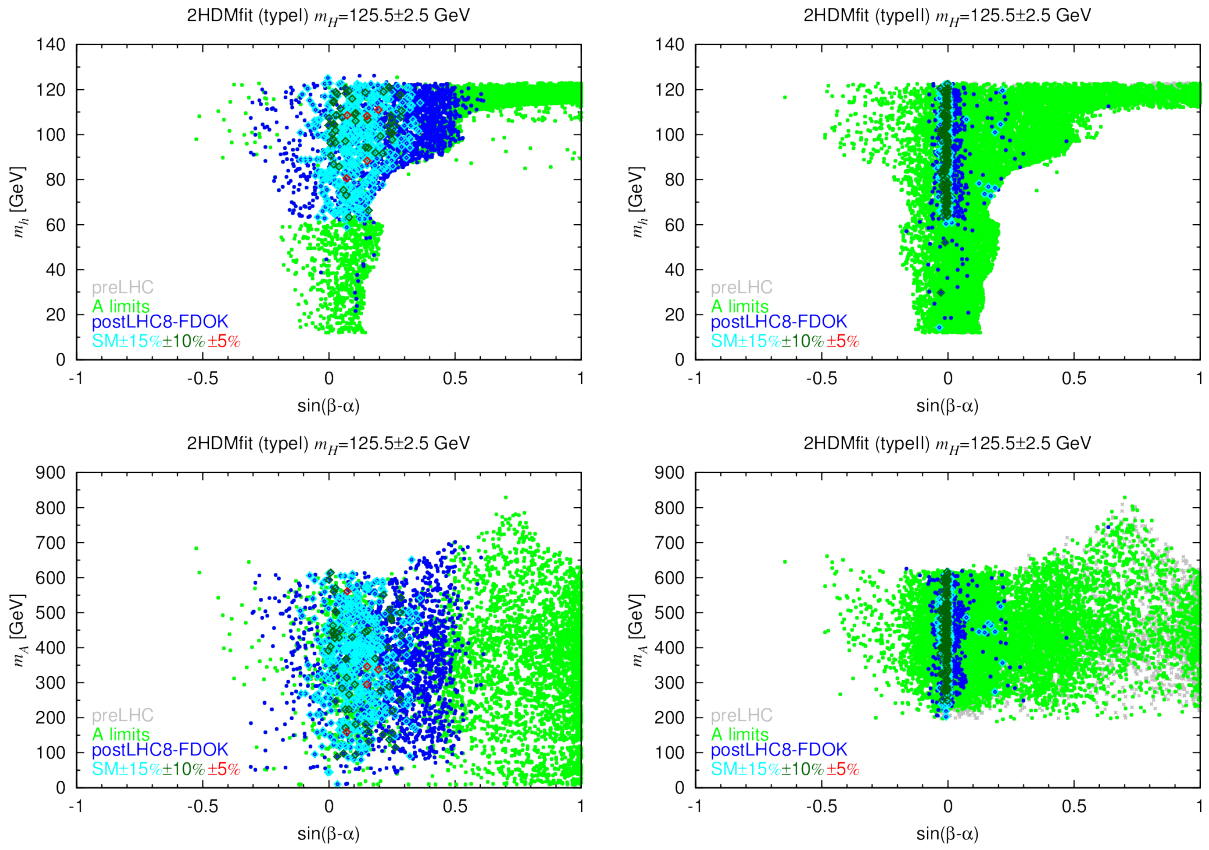

FIG. 22: Constraints in the m_h vs. $\sin(\beta-\alpha)$ and m_A vs. $\sin(\beta-\alpha)$ planes for the $m_H \sim 125.5$ GeV scenarios. Results for $m_{H^\pm}$ vs. $\sin(\beta-\alpha)$ are very similar to those for m_A vs. $\sin(\beta-\alpha)$. There are no FDOK requirements imposed on the preLHC and A-limits points. The SM$\pm 15\%, \pm 10\%, \pm 5\%$ points *are* subjected to FDOK requirements.

Let us now address the issue of feed down. Given that m_A can be quite large, there is certainly the possibility of $A \to ZH$ feed down contributions to the H signals. The HAZ coupling is proportional to $\sin(\beta-\alpha)$, which the fits require to be $\lesssim 0.5$ in magnitude. What is important, however, is $\mathrm{BR}(A \to ZH) = \Gamma(A \to ZH)/\Gamma_{\rm tot}(A)$, which can still be large. Figure 23 shows the FD μ values analogous to those considered for the $m_h \sim 125.5$ GeV scenario. To be precise, we consider

$$\mu^{\rm FD}_{{\rm ggF}H+{\rm bb}H} \equiv \frac{(\sigma_{{\rm ggF}A}+\sigma_{{\rm bb}A})\,P_{\rm FD}(A\to H+X)}{\sigma_{{\rm ggF}H}+\sigma_{{\rm bb}H}}\,, \tag{9}$$

$$\mu^{\rm FD}_{ZH} \equiv \frac{\sigma_{{\rm ggF}A}\mathrm{BR}(A\to ZH)}{\sigma_{ZH}}\,. \tag{10}$$

We observe that substantial FD is indeed possible. The ratio defining $\mu^{\rm FD}_{ZH}$ above, has

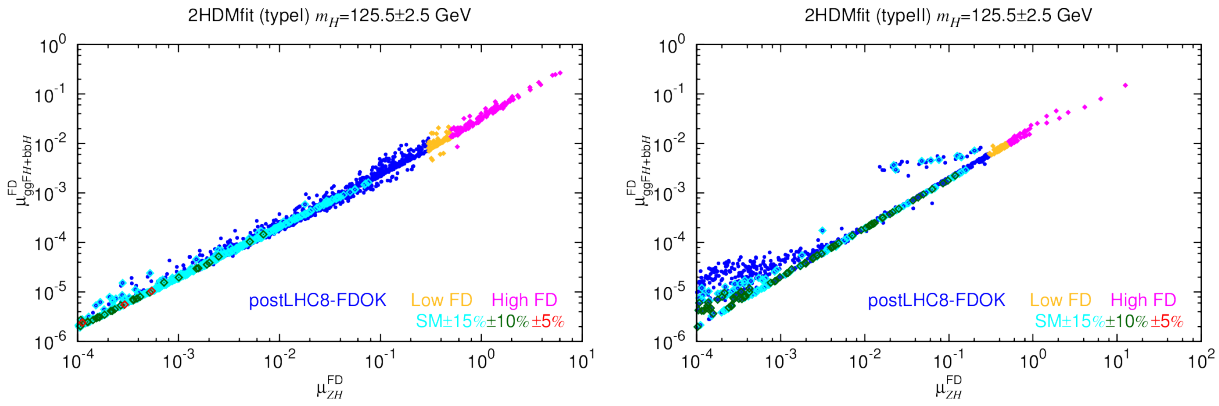

FIG. 23: We plot $\mu^{\rm FD}_{{\rm ggF}H+{\rm bb}H}$ vs. $\mu^{\rm FD}_{ZH}$ illustrating how high FD fractions can go for postLHC8 points for the $m_H \sim 125.5$ GeV scenarios. Also shown is how convergence of the H properties to SM-like values would limit the maximum possible feed downs. We display only points with $\mu^{\rm FD}_{ZH} \geq 10^{-4}$ — there are many points with much lower values.

the greatest potential for being large because of the large $gg \to A$ production rate in the numerator compared to the $Z^* \to ZH$ rate appearing in the denominator. In contrast, in $\mu^{\rm FD}_{{\rm ggF}H+{\rm bb}H}$ both numerator and denominator are ggF-dominated. As in the $m_h = 125.5$ GeV case, we exclude from subsequent plots those points which have FD levels that exceed 10% relative to the $gg \to H + bbH$ production modes and 30% in the ZH associated production mode.

As in the case of $m_h \sim 125.5$ GeV, it is interesting to assess the prospects for detecting a deviation in the triple-Higgs coupling as one goes from the current data set to H rates that are increasingly SM-like. In Fig. 24, we plot ${\rm sgn}(C_V^H)C_{HHH}$, *i.e.* the ratio of the triple-Higgs coupling λ_{HHH} to the value it should have in the SM limit, as a function of m_A. [We include ${\rm sgn}(C_V^H)$ because some of the points have $C_V^H < 0$ for our scanning procedure.] We observe that as the LHC signals become increasingly SM-like, the deviations of ${\rm sgn}(C_V^H)C_{HHH}$ from unity are even more tightly limited than in the case of C_{hhh} for $m_h \sim 125.5$ GeV. Of course, we also see (again) that very few (no) points survive the SM±5% constraint in the case of Type I (Type II).

Let us next assess the feasibility for detecting the lighter h. As already noted, finding points with $m_h \lesssim 60$ GeV for which ${\rm BR}(H \to hh)$ is small enough to still allow the H rates in the various channels to fit the 125.5 GeV signal is highly nontrivial and this scenario

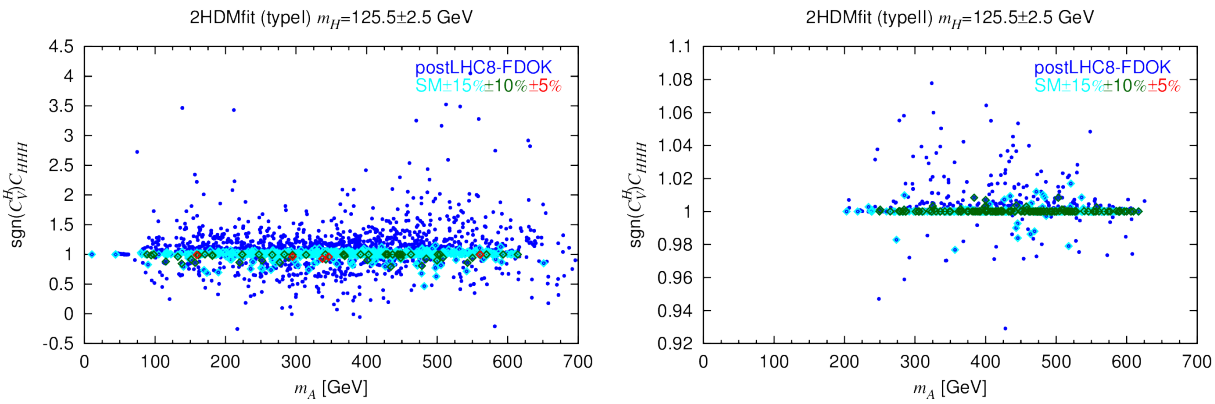

FIG. 24: We display points in the sgn$(C_V^H)C_{HHH}$ vs. m_A plane for the $m_H \sim 125.5$ GeV scenario comparing current H fits to the case where future measurements show that *all* channel rates are within $\pm 15\%, \pm 10\%, \pm 5\%$ of the SM Higgs prediction; FDOK is required in all cases. Color scheme is as for Fig. 19, except that preLHC and A-limits points are not displayed.

will be discussed in detail elsewhere. The most interesting modes for h detection may be $gg \to h \to \gamma\gamma$ and V^*h with $h \to b\bar{b}$. In the context of the current 8 TeV data, only the latter mode is of interest — expected signal strengths as a function of m_h are plotted in Fig. 25. While for many points the expected rates are obviously too small to have allowed detection of the h, there also exist postLHC8-FDOK points for which detection in the $Vh(b\bar{b})$ final state might be on the edge. We speculate that for the $Vh(b\bar{b})$ final state, a leptonic trigger on the V might still allow the predicted signal to emerge for the higher $\mu^h_{\rm VH}(b\bar{b})$ values.

As an aside, it is easily inferred from Fig. 25 that the postLHC8 and, even more so, the SM$\pm 15\%, \pm 10\%, \pm 5\%$ requirements eliminate a large swath of the points that survive the A-limits constraint. It is also noteworthy that in the case of Type I all preLHC points automatically satisfy the A-limits requirement, whereas some preLHC (grey) points get excluded by the A limits in the case of Type II.

Considering Fig. 25, it is moreover interesting to ask whether the $\gtrsim 2\sigma$ LEP excess in the $Zb\bar{b}$ final state at $M_{b\bar{b}} \sim 98$ GeV could be explained by $m_h \sim 98$ GeV and $\mu^h_{\rm VH}(b\bar{b}) \sim 0.1-0.3$. We see that this is indeed possible in both the Type I and Type II models given current postLHC8 constraints on the H properties. Of course, the scatterplots suggest that this explanation is more fine-tuned in the Type II case. Furthermore, if the H rates are found to be within $\pm 15\%$ of the SM rates, the value of $\mu^h_{\rm VH}(b\bar{b})$ is pushed well below the desired

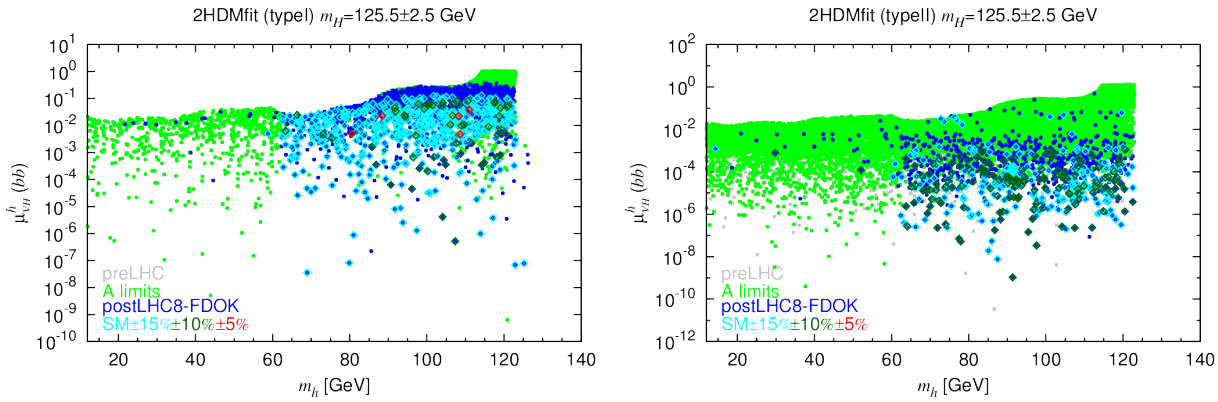

FIG. 25: $\mu^h_{\rm VH}(b\bar{b})$, *i.e.* $V^* \to Vh$ associated production with $h \to b\bar{b}$ relative to the SM, as a function of m_h. Note that $\mu^h_{\rm VH}(bb)$ is actually independent of energy and that the ratio also applies to any situation where the subprocess of interest is $V^* \to Vh$, including the LEP $Z^* \to Zh$ process. There are no FDOK requirements imposed on the preLHC and A-limits points. The SM$\pm$15%, $\pm$10%, $\pm$5% points *are* subjected to FDOK requirements.

range in the case of Type II and is at a marginal level in the case of Type I. At the SM$\pm$5% level, the few surviving Type I points have $\mu^h_{\rm VH}(b\bar{b}) \lesssim 0.05$ (assuming that a more extensive scan would reveal red points with $m_h \sim 98$ GeV that would have a signal level comparable to those around 90 GeV and 108 GeV plotted), a value that is not very consistent with the LEP $\sim 2.3\sigma$ excess observed.

At 14 TeV, there is also potential for detecting the h in the $gg \to h \to \gamma\gamma$ mode, as shown in Fig. 26. Of course, while a significant event yield is possible for $L \geq 300$ fb^{-1}, the level of continuum irreducible and reducible backgrounds must be assessed and could prove too large for the blip at m_h to be observable.

Finally, let us turn to the question of detecting the pseudoscalar A. Figure 27 shows cross sections for pseudoscalar A production, concretely $[\sigma(gg \to A) + \sigma(bbA))] \times {\rm BR}(A \to \gamma\gamma)$ (top), $\times\, {\rm BR}(A \to \tau\tau)$ (middle) and $\times\, {\rm BR}(A \to t\bar{t})$ (bottom) at 14 TeV as a function of m_A.[7] Again, there is a large range of possible cross section values at any given m_A, with the $\tan\beta$ dependence, of course, being the same as for the $m_h \sim 125.5$ GeV case. As already observed in Fig. 20, the possible range of m_A is limited when $m_H \sim 125.5$ GeV.

[7] As commented in the last section, we plot the sum as this defines the inclusive production rate. Of course, separating $gg \to A$ and bbA production processes would eventually be possible.

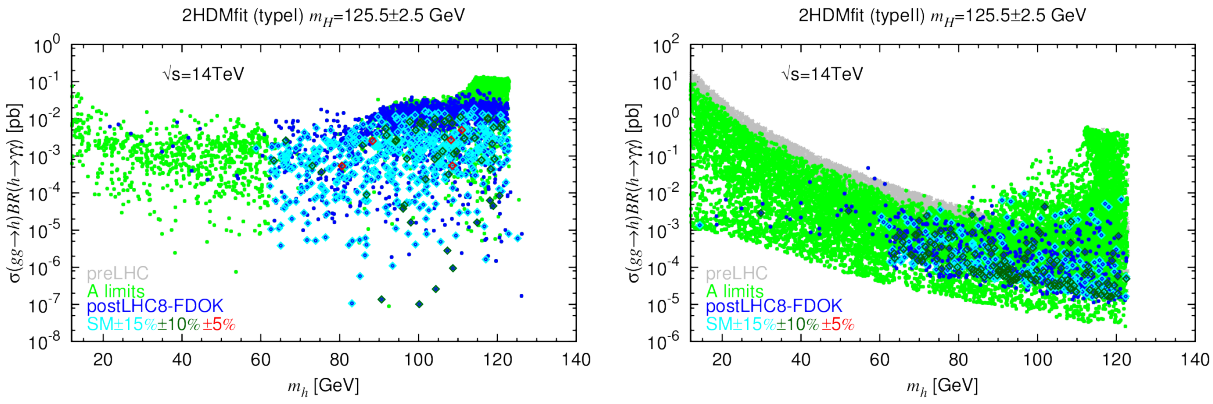

FIG. 26: $\sigma(gg \to h)\mathrm{BR}(h \to \gamma\gamma)$ for $\sqrt{s} = 14$ TeV with postLHC8-FDOK constraints imposed as well as further limitations imposed by SM$\pm$15%, $\pm$10%, $\pm$5% constraints. There are no FDOK requirements imposed on the preLHC and A-limits points. The SM$\pm$15%, $\pm$10%, $\pm$5% points *are* subjected to FDOK requirements.

In the case of Type II models, $m_A \lesssim 200$ GeV is eliminated due to the B-physics limit of $m_{H^\pm} \gtrsim 300$ GeV and the requirement of an acceptable T parameter (which limits the $A-H^\pm$ mass difference). In the case of Type I models, $m_A \lesssim 60$ GeV is possible but finding points with small enough $H \to AA$ to allow the H to have reasonably SM-like properties requires significant fine-tuning. For most m_A, the Type II maximal and minimal cross sections tend to be substantially (by a factor of > 1000) larger than for Type I. The lowest cross section values in Type I models are really very small at the largest allowed m_A values and would not allow the detection of the A boson. In contrast, in Type II models, even the very lowest cross section value of $\sim 5 \times 10^{-5}$ pb at $m_A \sim 630$ GeV would imply a handful of events for $L = 300$ fb^{-1}. The maximum Type II values imply a substantial number of events at all m_A, even at the largest masses, $m_A \sim 630$ GeV. [We remind the reader that 630 GeV is the upper limit allowed by perturbativity once the precision Higgs constraints, which limit $|\sin(\beta-\alpha)|$ to smaller values, have been included, cf. Fig. 20.]

As before, the rates for A production in the $\mu\mu$ final state are simply obtained by the $\tan\beta$-independent rescaling factor $\mathrm{BR}(A \to \mu\mu)/\mathrm{BR}(A \to \tau\tau) \sim 3.5 \times 10^{-3}$. For $m_A \lesssim 2m_t$, the cross section values near the upper limit obtained from such rescaling of the $\tau\tau$ final state rates shown in Fig. 27 are likely to be observable given the relatively narrow nature of the mass peak (typically of order a few GeV) and the excellent $\mu\mu$ invariant mass resolution.

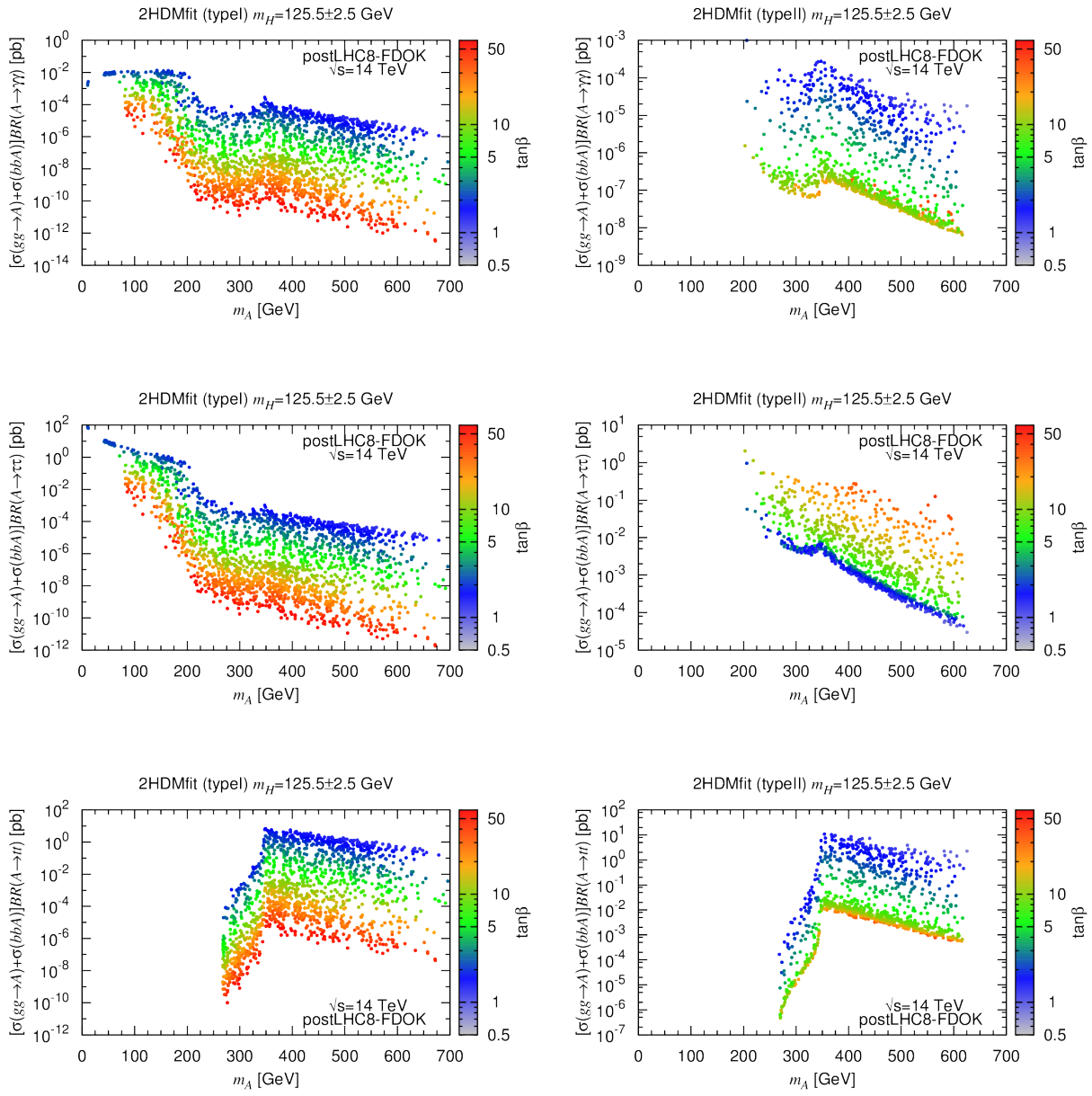

FIG. 27: Rates (in pb) of pseudoscalar A production at $\sqrt{s} = 14$ TeV as a function of m_A for the $m_H \sim 125.5$ GeV scenarios, separated into different A decay modes: $A \to \gamma\gamma$ (top), $A \to \tau\tau$ (middle) and $A \to t\bar{t}$ (bottom). In each case, we sum over $gg \to A$ and $gg \to bbA$ production. The values of $\tan\beta$ are color-coded as indicated by the scale on the right of the plots.

Last but not least, an interesting question is whether the h, A (and $H^\pm$) could *all* escape detection for some parameter choices when $m_H \sim 125.5$ GeV. Given the upper limit discussed above of $m_A \lesssim 630$ GeV (after Higgs fitting constraints), a careful examination is

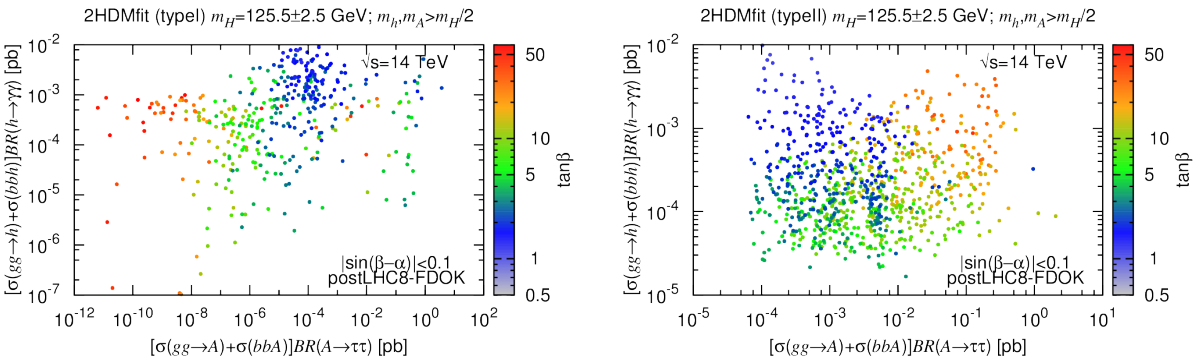

FIG. 28: We plot $[\sigma(gg \to h) + \sigma(bbh)]\mathrm{BR}(h \to \gamma\gamma)$ vs. $[\sigma(gg \to A) + \sigma(bbA)]\mathrm{BR}(A \to \tau\tau)$ for $\sqrt{s} = 14$ TeV with postLHC8-FDOK constraints imposed. Colors indicate the value of $\tan\beta$. We have required $|\sin(\beta - \alpha)| < 0.1$ so that the rate for $V^* \to Vh$ will be at most 0.01 times the SM rate at the same mass.

required.

Consider first the A. In the case of Type I, Fig. 27 shows that for $m_A \in [200, 300]$ GeV (and most probably all the way out to the maximum allowed m_A) and large $\tan\beta$ the $\gamma\gamma, \tau\tau, t\bar{t}$ rates are all very small and would not allow discovery of the A even with $L = 3000$ fb^{-1}. In the case of Type II, the anticorrelation between the $\tau\tau$ and $t\bar{t}$ rates as $\tan\beta$ is varied, combined with the relatively substantial $\tau\tau$ rates for m_A below the $t\bar{t}$ threshold combine to guarantee that the A should be detectable with $L = 3000$ fb^{-1} in either the $\tau\tau$ or the $t\bar{t}$ mode, and perhaps in both.

As regards the h, it is first of all clear that if $|\sin(\beta - \alpha)|$ is very small (as certainly both allowed and preferred by Higgs fitting) then the $V^* \to Vh$ rates will be very tiny, as illustrated in Fig. 25 in the $m_h > 60$ GeV region for both Type I and Type II. The other potentially viable mode is $gg \to h \to \gamma\gamma$. However, Fig. 26 shows very small rates in this case as well for Type I. In contrast, the lowest cross sections in this channel in Type II are of order 10^{-5} pb, a level which might be accessible with $L = 3000$ fb^{-1}.

To summarize the above, in Type II $m_H \sim 125.5$ GeV scenarios, the prospects for the discovery of the A boson are very good, and there is an excellent chance of finding the h as well in the $\gamma\gamma$ final state. In contrast, in Type I there are clearly regions of parameter space for which no Higgs boson other than the SM-like H will be discoverable without going

to still higher luminosity or energy. These results are summarized in Fig. 28 where we see from the right-hand plot that in Type II both the h and A have an excellent chance of being detectable in the $\gamma\gamma$ and $\tau\tau$ modes, respectively. In contrast, the left-hand plot shows that there is clearly a corner of parameter space where detection of both the h and the A will be extremely challenging. Of course, we have not explored prospects for $H^\pm$ discovery in this paper, but its production cross sections are typically substantially below those for the A since $H^\pm$ production requires at least one top quark in the final state.

Finally, we note the regions with $m_A \sim 200 - 350$ GeV and low $\tan\beta$ of the $\gamma\gamma$ and $\tau\tau$ final state Type I plots that have been depleted by the removal of points with excessive feed down. These regions are, of course, the analogue of the FD-depleted regions discussed in the case of $m_h \sim 125.5$ GeV.

V. CONCLUSIONS

The latest Higgs data from the LHC clearly favor a fairly SM-like Higgs boson with mass of about 125.5 GeV. In this paper we have quantified this in the context of Type I and Type II 2HDMs, identifying either the h or the H as the 125.5 GeV state. Indeed, the vector boson pair coupling of the 125.5 GeV state must be quite close to the SM Higgs coupling, but at low $\tan\beta$ there is significant dispersion about the SM values for the fermionic couplings. Given the constraints on the 125.5 GeV state, we have ascertained expectations for the other Higgs bosons H, $H^\pm$ and A in the case that it is the h that gives the SM-like signal. We demonstrated that there are many parameter space points (satisfying all 95% C.L. constraints on the h) that for $\sqrt{s} = 14$ TeV could allow for observation of the H and A in a variety of modes, including not just the ZZ (for H only), $\tau\tau$ and $t\bar{t}$ final states, but also $\mu\mu$ and $\gamma\gamma$. In the $m_H \sim 125.5$ GeV case, the A can also be detected in these same modes (except ZZ). In addition, there is good probability for viable signals for the lighter h. In particular, the $V^* \to Vh$ with $h \to b\bar{b}$ channel might yield a detectable signal for at least a fraction of the points surviving the 95% C.L. limits on the H signal at 125.5 GeV.

Nondecoupling of the charged-Higgs loop contribution to the $h\gamma\gamma$ or $H\gamma\gamma$ coupling plays an important role once rates are required to be within $\pm 5\%$ of the SM predictions. The result is elimination of all but a tiny fraction of the $m_H \sim 125.5$ GeV Type I scenarios and *all* of the $m_H \sim 125.5$ GeV Type II scenarios as well as *all* of the wrong-sign Yukawa Type II

scenarios in the $m_h \sim 125.5$ GeV case.

Along the way, we clarified the important role played by constraints deriving from requirements of perturbativity in reducing the otherwise huge parameter space of the 2HDMs. We also delineated the (fortunately) rather limited impact of removing points that suffer from a large amount of feed down from heavier Higgs bosons decaying either directly or via chain decay to a final state containing the 125.5 GeV state.

An important general conclusion is that even if the 125.5 GeV signal rates converge to very SM-like values, the 2HDMs predict ample opportunity for detecting the other Higgs bosons. Still, it is also true that in the case of $m_h \sim 125.5$ GeV in the decoupling limit of very large $m_A \sim m_H \sim m_{H^\pm}$ detection of even one of the other Higgs bosons at LHC14 would not be possible. However, the case of $m_H \sim 125.5$ GeV is different. Because the maximum m_A is limited, having the h, A and $H^\pm$ all escape detection is very unlikely in Type II 2HDM. However, in Type I if $m_A \in [200, 300]$ GeV and $\tan\beta$ is large, then the A will not be detectable and h detection will be very marginal.

Finally, we make special note of the scenarios with low $m_A < 100$ GeV that escape all LEP and (so far) LHC limits and yet have quite substantial $gg \to A$ and bbA production cross sections. It will be interesting to probe these scenarios, which are possible for both Type I and Type II in the $m_h \sim 125.5$ GeV case and for Type I in the $m_H \sim 125.5$ GeV case, in ongoing analyses of LHC 8 TeV data and in future LHC running at higher energy.

VI. ACKNOWLEDGEMENTS

This work was supported in part by U.S. DOE Grant No. DE-SC-000999 and by IN2P3 under PICS FR–USA Contract No. 5872. Y.J. is also supported by LHC-TI fellowship US NSF Grant No. PHY-0969510. In addition, he thanks the "Investissements davenir, Labex ENIGMASS" for partial financial support for a research stay at LPSC Grenoble. J.F.G. and S.K. thank the Aspen Center for Physics, supported by the National Science Foundation under Grant No. PHYS-1066293, for hospitality.

Appendix A: Generic formalism for feed down processes

We have quantitatively computed feed down as follows. Let us define the final state of interest by $Y = \gamma\gamma, VV, b\bar{b}, \tau\tau$ (the only final states quantitatively of relevance for fitting the ~ 125.5 GeV signal using the 7 + 8 TeV data set). The production processes will be denoted by XH =ggFH (standing for $gg \to$H), bbH (standing for associated production of the H with a $b\bar{b}$ pair), ttH, VBFH (standing for $WW/ZZ \to$ H), and VH. (Note that the regular Roman H is generic and we will be using these production processes for various different choices of H.) In this paper, we will consider ggFH and bbH together and compute their combined feed down. We wish to consider the feed down into $\mathbf{H} = h$ and H where $\mathbf{H}$ is always the 125.5 GeV state. In the process, we will have to consider production of all Higgses that are heavier than the $\mathbf{H}$, which Higgses we will denote by $\mathcal{H}$.

For all but VH, we can define the fraction of feed down contributing to production mode X as

$$\mu^{\rm FD}_{X\mathbf{H}} \equiv \frac{\sum_{\mathcal{H}} \sigma_{X\mathcal{H}} P_{\rm FD}(\mathcal{H} \to \mathbf{H} + \text{anything})}{\sigma_{X\mathbf{H}}} \,. \tag{A1}$$

Note that we have cancelled a common factor of BR($\mathbf{H} \to Y$), the branching ratio for $\mathbf{H}$ to decay to any final state $Y = \gamma\gamma, VV, b\bar{b}, \tau\tau$, that is common to the numerator and denominator. In the above, we have to take into account the possibilities that the intermediating $\mathcal{H}$ can decay to two $\mathbf{H}$'s or only one $\mathbf{H}$. Thus, we actually have

$$P_{\rm FD}(\mathcal{H} \to \mathbf{H} + \text{anything}) = 2P_{\mathcal{H},2\mathbf{H}} + P_{\mathcal{H},1\mathbf{H}} \,, \tag{A2}$$

so that in the first case the "anything" includes the 2nd $\mathbf{H}$. For 2$\mathbf{H}$ final states we include a multiplicative factor of 2 since both of the final $\mathbf{H}$'s will contribute. The formulas for the various $P_{\mathcal{H},2\mathbf{H}}$ and $P_{\mathcal{H},1\mathbf{H}}$'s cases can be found in [31] which we will repeat in the following context (including some corrections we found).

The VH process must be handled differently due to the fact that it is directly impacted by $gg \to A$ and bbA production with $A \to Z\mathbf{H}$ in the case of $V = Z$ and by $gg \to tbH^{\pm} \to tbW^{\pm}\mathbf{H}$ in the case of $V = W$. The largest of these fractional contaminations is that associated with $gg \to A + bbA$ since the cross sections for $H^{\pm}$ production are quite a bit smaller. In the $V = Z$ case, the leading contribution to the fractional feed down is

$$\mu^{\rm FD}_{Z\mathbf{H}} = \frac{[\sigma_{\rm ggF}A + \sigma_{\rm bbA}]{\rm BR}(A \to Z\mathbf{H})}{\sigma_{\rm Z\mathbf{H}}} \,, \tag{A3}$$

where the BR($\mathbf{H} \to Y$) branching ratios in numerator and denominator have once again cancelled and $\sigma_{\mathbf{ZH}}$ is that arising from the $Z^* \to Z\mathbf{H}$ subprocess. In the above, we have neglected (a good approximation) contributions to the $Z\mathbf{H}$ + anything final state due to the FD processes other than the direct $gg \to A \to Z\mathbf{H}$ production process. In particular, we neglect the terms which lead to final states containing $Z\mathbf{H}$ plus additional particles. Besides yielding small contributions to $\mu^{\rm FD}_{V\mathbf{H}}$, such terms yield final states that are much more complicated than the simple $Z\mathbf{H}$ final state, containing, for example, more than one Z or a $Z + W$ pair. The selection criteria for the $Z\mathbf{H}$ final state are likely to be such that these more complicated final states were discarded or strongly discriminated against. In the following subsections, we apply these general formulas to the two 2HDM scenarios discussed in this paper, showing how to determine the magnitude of feed down associated with a given point in parameter space.

Example I: Feed down of heavier Higgs bosons to a 125.5 GeV h

In this case, the $\mathbf{H} = h$ can be produced from the chain decay of heavier Higgs bosons $\mathcal{H} = H, A, H^\pm$. Since the cross section for $gg \to tbH^\pm$ is relatively smaller than those for H and A (because of the t in the $tbH^\pm$ final state), we will not include $H^\pm$ as an intermediate source for the FD mechanism. In practice, important FD contributions arise from (ggF+bb)H, (ggF+bb)A or VBFH. The most important feed down decays for ggF+bb are $H \to hh$ and $A \to Zh$ (or $A \to ZH$ for the case of $m_H \sim 125.5$ GeV) and for VBF $H \to hh$. However, the approximations of

$$P_{H,2h} \simeq \mathrm{BR}(H \to hh)\,, \quad P_{A,1h} \simeq \mathrm{BR}(A \to Zh)\,, \tag{A4}$$

are not generally adequate.

It is convenient to consider separately the chains that can yield $2h$ in the final state vs. those that yield only $1h$ in the final state. Some sample net branching ratios, denoted (following [31]) by P are the following. First, if H is the primary then $H \to AA$ and

$H \to H^+H^-$ are possible for some 2HDM points in addition to $H \to hh$. Thus, we have

$$\begin{aligned} P_{H,2h} &= \mathrm{BR}(H \to hh) + \mathrm{BR}(H \to H^+H^-)\big[\mathrm{BR}(H^+ \to W^+h)^2 \\ &\quad + \mathrm{BR}(H^+ \to W^+A)^2\mathrm{BR}(A \to Zh)^2 \\ &\quad + 2\mathrm{BR}(H^+ \to W^+h)\mathrm{BR}(H^+ \to W^+A)\mathrm{BR}(A \to Zh)\big] \\ &\quad + \mathrm{BR}(H \to AA)\big[\mathrm{BR}(A \to Zh)^2 + 4\mathrm{BR}(A \to W^-H^+)^2\mathrm{BR}(H^+ \to W^+h)^2 \\ &\quad + 4\mathrm{BR}(A \to Zh)\mathrm{BR}(A \to W^-H^+)\mathrm{BR}(H^+ \to W^+h)\big]\,, \end{aligned} \tag{A5}$$

$$\begin{aligned} P_{H,1h} &= \mathrm{BR}(H \to ZA)\mathrm{BR}(A \to Zh) + 2\mathrm{BR}(H \to W^-H^+)\mathrm{BR}(H^+ \to W^+h) \\ &\quad + 2\mathrm{BR}(H \to H^+H^-)\big[\mathrm{BR}(H^+ \to W^+h) \\ &\quad + \mathrm{BR}(H^+ \to W^+A)\mathrm{BR}(A \to Zh)\big]p(H^+ \not\to h) \\ &\quad + \mathrm{BR}(H \to AA)\big[2\mathrm{BR}(A \to Zh) + 4\mathrm{BR}(A \to W^-H^+)\mathrm{BR}(H^+ \to W^+h)\big]p(A \not\to h)\,, \end{aligned} \tag{A6}$$

where

$$\begin{aligned} p(H^+ \not\to h) &= 1 - \mathrm{BR}(H^+ \to W^+h) - \mathrm{BR}(H^+ \to W^+A)\mathrm{BR}(A \to Zh)\,, \\ p(A \not\to h) &= 1 - \mathrm{BR}(A \to Zh) - 2\mathrm{BR}(A \to W^-H^+)\mathrm{BR}(H^+ \to W^+h)\,. \end{aligned} \tag{A7}$$

If A is the primary then possibly accessible modes at the first stage are $A \to ZH$, and $A \to W^+H^-, W^-H^+$, resulting in

$$P_{A,2h} = \mathrm{BR}(A \to ZH)\overline{P}_{H,2h} + 2\mathrm{BR}(A \to W^-H^+)\mathrm{BR}(H^+ \to W^+H)\mathrm{BR}(H \to hh)\,, \tag{A8}$$

$$\begin{aligned} P_{A,1h} &= \mathrm{BR}(A \to Zh) + \mathrm{BR}(A \to ZH)\overline{P}_{H,1h} \\ &\quad + 2\mathrm{BR}(A \to W^-H^+)\mathrm{BR}(H^+ \to W^+h)\,, \end{aligned}$$

where the appropriate expressions for the two P's are the same as given earlier with the A channels eliminated since H being a secondary particle must be lighter than the A.

$$\begin{aligned} \overline{P}_{H,2h} &= \mathrm{BR}(H \to hh) + \mathrm{BR}(H \to H^+H^-)\mathrm{BR}(H^+ \to W^+h)^2\,, \\ \overline{P}_{H,1h} &= 2\mathrm{BR}(H \to W^-H^+)\mathrm{BR}(H^+ \to W^+h) \\ &\quad + 2\mathrm{BR}(H \to H^+H^-)\mathrm{BR}(H^+ \to W^+h)p(H^+ \not\to h)\,. \end{aligned} \tag{A9}$$

For the sake of completeness, we also provide the formula for the case that H^+ or H^- is produced as the primary Higgs. In this case, the first level decays of relevance are $H^+ \to$

W^+h and $H^+ \to W^+H$, leading to

$$P_{H^+,2h} = \mathrm{BR}(H^+ \to W^+H)P_{H,2h} + \mathrm{BR}(H^+ \to W^+A)\mathrm{BR}(A \to ZH)\mathrm{BR}(H \to hh)\,, \quad \text{(A10)}$$
$$P_{H^+,1h} = \mathrm{BR}(H^+ \to W^+h) + \mathrm{BR}(H^+ \to W^+H)P_{H,1h} + \mathrm{BR}(H^+ \to W^+A)\mathrm{BR}(A \to Zh)\,,$$

where the $P_{H,2h}$ and $P_{H,1h}$ are as given earlier in Eqs. (A5) and (A6), respectively, with kinematics for the H^+ primary situation eliminating the terms involving $H \to W^-H^+$ and $H \to H^+H^-$.

Furthermore, in order to illustrate the importance of keeping the full formulas we show in Fig. 29 the fraction of $1h$ final states coming directly from $A \to Zh$ vs. the fraction of $2h$ final states coming directly from $H \to hh$.

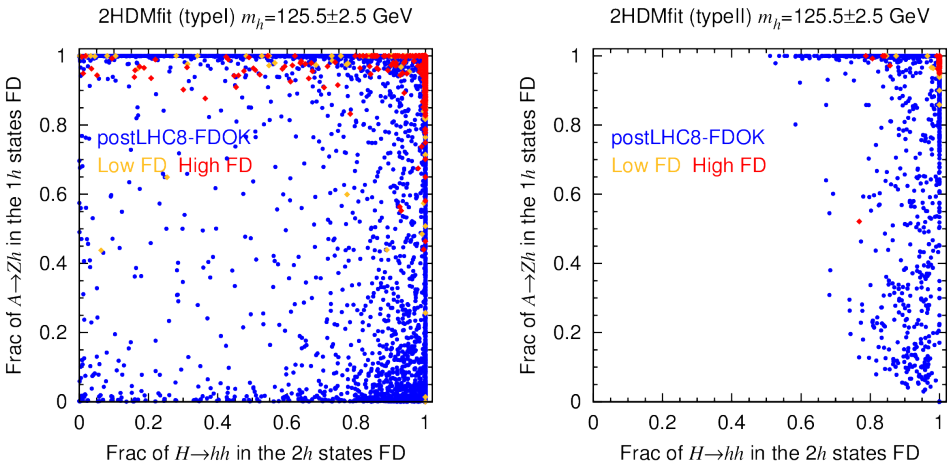

FIG. 29: We plot $[\sigma(gg \to H + bbH)2\mathrm{BR}(H \to hh)]/[\sigma(gg \to H + bbH)2P_{H,2h} + \sigma(gg \to A + bbA)2P_{A,2h}]$ on the x axis and $[\sigma(gg \to A + bbA)\mathrm{BR}(A \to Zh)]/[\sigma(gg \to H + bbH)P_{H,1h} + \sigma(gg \to A + bbA)P_{A,1h}]$ on the y axis. The postLHC8-FDOK points are displayed in blue. The cyan, green and red points obey FDOK constraints and have all the channel rates of Eq. (6) within SM±15%, SM±10% and SM±5%, respectively; cf. Fig. 7.

Example II: Feed down of heavier Higgs to a 125.5 GeV H

The case of $\mathbf{H} = H$ in the 2HDM is much simpler. Ignoring the $H^\pm$ as explained above, the only heavier Higgs which can feed the H signal is $\mathcal{H} = A$. Therefore, the most important FD processes are $gg \to A + bbA$ with $A \to ZH$. However, the approximations of

$$P_{A,1H} \simeq \mathrm{BR}(A \to ZH)\,, \quad \text{(A11)}$$

are not generally applicable. In order to measure the FD precisely, one should use the full expression for $P_{A,2H}$ and $P_{A,1H}$ as follows

$$P_{A,2H} = \mathrm{BR}(A \to H^+H^-)\mathrm{BR}(H^+ \to W^+H)^2\,, \tag{A12}$$
$$P_{A,1H} = \mathrm{BR}(A \to ZH) + 2\mathrm{BR}(A \to W^-H^+)\mathrm{BR}(H^+ \to W^+H) + 2\mathrm{BR}(A \to H^+H^-)\mathrm{BR}(H^+ \to W^+H)p(H^+ \not\to H)\,,$$

where

$$p(H^+ \not\to H) = 1 - \mathrm{BR}(H^+ \to W^+H)\,. \tag{A13}$$

Appendix B: Nondecoupling of the $H^\pm$ loop contribution to the $H\gamma\gamma$ coupling and wrong-sign Yukawa effects on the ggH coupling.

We have claimed that the $m_H = 125.5$ GeV Type II scenarios can be either eliminated or confirmed when the LHC measurements reach a precision such that the rates in the various initial×final state channels can be measured to 5% accuracy. As we have said, this is because for this scenario the charged Higgs loop does not decouple in the $H\gamma\gamma$ coupling calculation and results in at least a 5% reduction in the coupling relative to the SM prediction, *i.e.* in C_γ^H. This can easily be explained using the results of Appendix B of [41] as translated to the current situation.

We first emphasize that in all the fits, whether Type I or Type II, the LHC data require that the sign of the top-quark Yukawa, *i.e.* C_U^H, be the same as the sign of the HVV coupling C_V^H in order that the $\gamma\gamma$ final state rates not be too enhanced. Referring to Table I, we see that a SM-like H results in $\cos(\beta-\alpha) = \pm 1$, for which $C_U^H = \pm 1$, respectively. In our scan range of $|\alpha| \le \pi/2$ both signs are found. For Type I, C_U^H and C_D^H have the same sign. For Type II, C_D^H is always positive within the α scan range. Thus, in Type I we always have the same relative signs between all the couplings as for a SM Higgs boson, whereas in Type II there will be scan points for which C_D^H has the "wrong" sign relative to C_V^H and C_U^H. This will impact the ggH 1-loop coupling because the interference between the top-quark and bottom-quark loops will change sign, thereby increasing the ggH coupling by a factor of $C_g^H \sim 1.12$ relative to the SM value — see Appendix B of [41] — a level that can be probed in a future LHC run from the observation of the decay products of Higgs bosons originating from gluon fusion. In contrast, the change in sign of the bottom-quark loop contribution to

the $H\gamma\gamma$ coupling yields a $\lesssim 1\%$ decrease in C_γ^H due to the dominance of the W- and t-loop contributions. However, it turns out that for *all* of the Type II scenarios the charged-Higgs loop contribution to the $H\gamma\gamma$ coupling does not decouple as $m_{H^\pm}$ becomes large. As a result, all Type II scenarios with $m_H \sim 125.5$ GeV will be eliminated if future LHC data determine that C_γ^H is within 5% of the SM prediction of unity. This happens regardless of the common sign of C_V^H and C_U^H, denoted by $\mathrm{sgn}(C_V^H)$.

To gain intuition, we employ the results of [7] to find that in the limit where $\cos(\beta-\alpha) \to \pm 1$ the dimensionless HH^+H^- coupling takes the form

$$g_{HH^+H^-} = -\frac{\mathrm{sgn}(C_V^H)}{v^2}(m_H^2 + 2m_{H^\pm}^2 - 2\hat{m}_{12}^2)\,. \tag{B1}$$

Further, perturbativity requires that $\hat{m}_{12}^2$ be of modest size, and, of course, m_H is fixed at ~ 125.5 GeV. Thus, we have the asymptotic result that

$$\frac{v^2 g_{HH^+H^-}\,\mathrm{sgn}(C_V^H)}{m_{H^\pm}^2} \to -2\,. \tag{B2}$$

As shown in Appendix B of [41] for the case of $C_V^H > 0$ (but the same arguments apply with all signs changed to the $C_V^H < 0$ case[8]), this means that C_γ^H is reduced by 5% relative to the SM value of unity. Of course, $\hat{m}_{12}$ is not exactly zero, but one finds that $\hat{m}_{12}^2$ lies below $(100\text{ GeV})^2$ while being able to reach large negative values for a large range of $m_{H^\pm}$. The result is that $v^2 g_{HH^+H^-}\,\mathrm{sgn}(C_V^H)$ is always *at most* $-2m_{H^\pm}^2$, implying that the decrease in C_γ^H is at least 5%. This is illustrated in Fig. 30.

This Type II situation can be contrasted with Type I. As stated earlier, in Type I C_V^H, C_U^H and C_D^H all have the same sign, which can be either plus or minus with respect to the SM convention of $C_V^{H_{\rm SM}} = +1$. We plot in Fig. 31 the same quantities as in Fig. 30. We observe that the bulk of the parameter space, namely that portion with $C_D^H > 0$, has $v^2 g_{HH^+H^-}\,\mathrm{sgn}(C_V^H) \lesssim -2m_{H^\pm}^2$ leading to at least a 5% suppression of C_γ. In the other branch, we have $C_D^H < 0$. In the end, various effects are competing and $v^2 g_{HH^+H^-}\,\mathrm{sgn}(C_V^H) \gtrsim -2m_{H^\pm}^2$, with values near zero and positive values as well being possible. The result is that $C_\gamma^H \sim 1$ is achievable and a good fit to LHC data is possible, although quite rare within our scans.

[8] The b-quark loop, which does not change sign when $C_V^H < 0$, is negligible relative to other contributions.

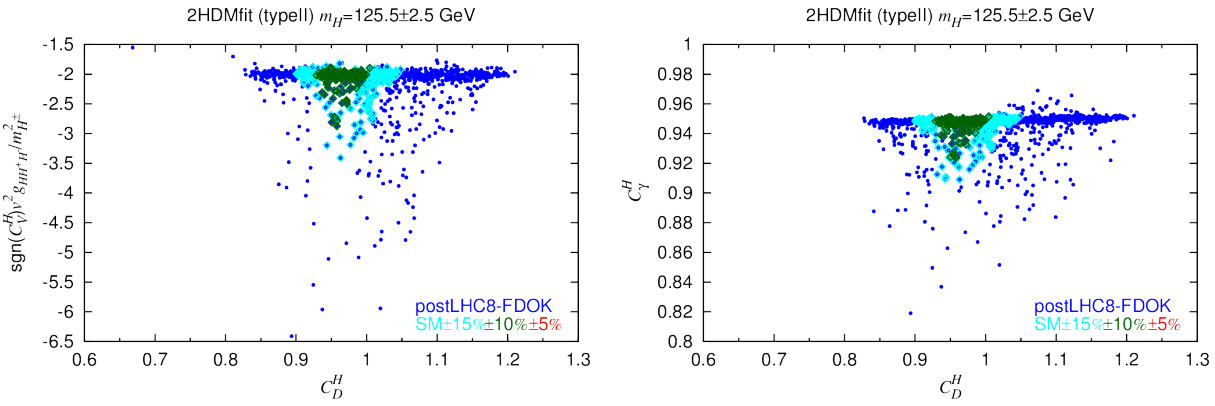

FIG. 30: For Type II 2HDM, we plot: $v^2 g_{HH^+H^-}\,\mathrm{sgn}(C_V^H)/m_{H^\pm}^2$ vs. C_D^H (left) and C_γ^H vs. C_D^H (right). We show FDOK points consistent at the postLHC8 level (blue) and after presumed LHC measurements showing SM consistency at the ±15% (cyan) and ±10% (dark green) level. No points survive if SM consistency is demonstrated at the ±5% level.

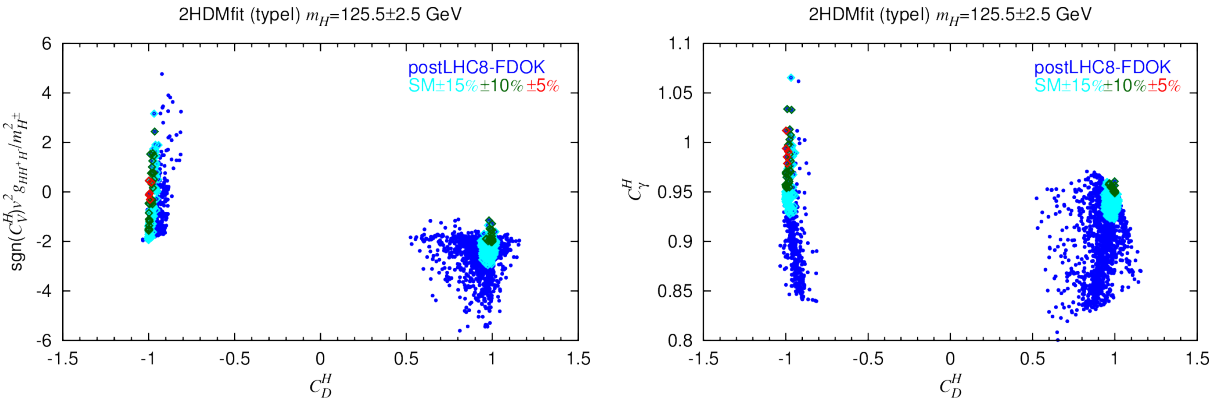

FIG. 31: For Type I 2HDM, we plot: Left, $v^2 g_{HH^+H^-}\,\mathrm{sgn}(C_V^H)/m_{H^\pm}^2$ vs. C_D^H (left) and C_γ^H vs. C_D^H (right), showing FDOK points consistent at the postLHC8 level (blue) and after presumed LHC measurements showing SM consistency at the ±15% (cyan), ±10% (dark green) and ±5% (red) levels.

A second means of discrimination relative to the SM arises in the context of the ggH coupling in the case of a Type II model. As noted above, in Type II C_D^H always has the same sign as in the SM, but C_U^H can have either the SM sign or a sign opposite the SM, *i.e.* $C_U^H \sim -1$. In this latter case, the sign of the interference terms between the top-quark and bottom-quark loop contributions to the ggH coupling changes. This results in a significant

increase of about 12% in the ggH coupling, as detailed in [41]. As also discussed there, C_g^H can eventually be measured to an accuracy of about 5% in future LHC runs as well as at a future linear collider, which would allow either confirmation or conflict with the $C_U^H \sim -1$ Type II case. In Fig. 32, we plot C_g^H as a function of C_U^H for both Type I and Type II models. There, we see that C_g^H is not generally a useful discriminator in the case of the Type I model nor on the $C_U^H \sim +1$ branch in the case of a Type II model.

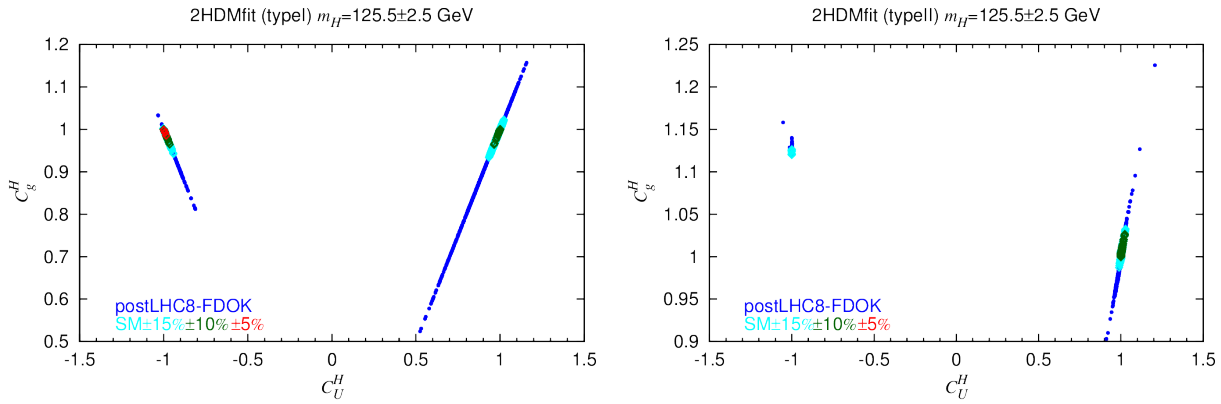

FIG. 32: We plot C_g^H vs. C_U^H for Type I (right) and Type II (left). We show FDOK points consistent at the postLHC8 level (blue) and after presumed LHC measurements showing SM consistency at the ±15% (cyan) and ±10% (dark green) levels. Points consistent with the SM (red points) at the ±5% level are only present in the $C_U^H < 0$ branch of the Type I model.

[1] **ATLAS** Collaboration, G. Aad et al., *Observation of a new particle in the search for the Standard Model Higgs boson with the ATLAS detector at the LHC*, *Phys.Lett.* **B716** (2012) 1–29, [arXiv:1207.7214].

[2] **CMS** Collaboration, S. Chatrchyan et al., *Observation of a new boson at a mass of 125 GeV with the CMS experiment at the LHC*, *Phys.Lett.* **B716** (2012) 30–61, [arXiv:1207.7235].

[3] **ATLAS** Collaboration, G. Aad et al., *Updated coupling measurements of the Higgs boson with the ATLAS detector using up to 25/fb of proton-proton collision data*, 2014. ATLAS-CONF-2014-009.

[4] **CMS** Collaboration, *Combination of standard model Higgs boson searches and measurements of the properties of the new boson with a mass near 125 GeV*, 2013. CMS PAS HIG-13-005.

[5] **ATLAS** Collaboration, G. Aad et al., *Measurements of Higgs boson production and couplings in diboson final states with the ATLAS detector at the LHC*, *Phys.Lett.* **B726** (2013) 88–119, [arXiv:1307.1427].

[6] J. F. Gunion, H. E. Haber, G. L. Kane, and S. Dawson, *THE HIGGS HUNTER'S GUIDE*, *Front.Phys.* **80** (2000) 1–448.

[7] J. F. Gunion and H. E. Haber, *The CP conserving two Higgs doublet model: The Approach to the decoupling limit*, *Phys.Rev.* **D67** (2003) 075019, [hep-ph/0207010].

[8] G. Branco, P. Ferreira, L. Lavoura, M. Rebelo, M. Sher, et al., *Theory and phenomenology of two-Higgs-doublet models*, *Phys.Rept.* **516** (2012) 1–102, [arXiv:1106.0034].

[9] C.-W. Chiang and K. Yagyu, *Implications of Higgs boson search data on the two-Higgs doublet models with a softly broken Z_2 symmetry*, *JHEP* **1307** (2013) 160, [arXiv:1303.0168].

[10] B. Grinstein and P. Uttayarat, *Carving Out Parameter Space in Type-II Two Higgs Doublets Model*, *JHEP* **1306** (2013) 094, [arXiv:1304.0028].

[11] B. Coleppa, F. Kling, and S. Su, *Constraining Type II 2HDM in Light of LHC Higgs Searches*, *JHEP* **1401** (2014) 161, [arXiv:1305.0002].

[12] O. Eberhardt, U. Nierste, and M. Wiebusch, *Status of the two-Higgs-doublet model of type II*, *JHEP* **1307** (2013) 118, [arXiv:1305.1649].

[13] S. Chang, S. K. Kang, J.-P. Lee, K. Y. Lee, S. C. Park, et al., *Two Higgs doublet models for the LHC Higgs boson data at $\sqrt{s} = 7$ and 8 TeV*, *JHEP* **1409** (2014) 101, [arXiv:1310.3374].

[14] K. Cheung, J. S. Lee, and P.-Y. Tseng, *Higgcision in the Two-Higgs Doublet Models*, *JHEP* **1401** (2014) 085, [arXiv:1310.3937].

[15] A. Celis, V. Ilisie, and A. Pich, *Towards a general analysis of LHC data within two-Higgs-doublet models*, *JHEP* **1312** (2013) 095, [arXiv:1310.7941].

[16] L. Wang and X.-F. Han, *Status of the aligned two-Higgs-doublet model confronted with the Higgs data*, *JHEP* **1404** (2014) 128, [arXiv:1312.4759].

[17] J. Baglio, O. Eberhardt, U. Nierste, and M. Wiebusch, *Benchmarks for Higgs Pair Production and Heavy Higgs Searches in the Two-Higgs-Doublet Model of Type II*, *Phys.Rev.* **D90** (2014) 015008, [arXiv:1403.1264].

[18] S. Inoue, M. J. Ramsey-Musolf, and Y. Zhang, *CPV Phenomenology of Flavor Conserving Two Higgs Doublet Models*, *Phys.Rev.* **D89** (2014) 115023, [arXiv:1403.4257].

[19] N. Craig, J. Galloway, and S. Thomas, *Searching for Signs of the Second Higgs Doublet*, arXiv:1305.2424.

[20] V. Barger, L. L. Everett, H. E. Logan, and G. Shaughnessy, *Scrutinizing the 125GeV Higgs boson in two Higgs doublet models at the LHC, ILC, and Muon Collider*, *Phys.Rev.* **D88** (2013) 115003, [arXiv:1308.0052].

[21] M. Carena, I. Low, N. R. Shah, and C. E. Wagner, *Impersonating the Standard Model Higgs Boson: Alignment without Decoupling*, *JHEP* **1404** (2014) 015, [arXiv:1310.2248].

[22] C.-Y. Chen, S. Dawson, and M. Sher, *Heavy Higgs Searches and Constraints on Two Higgs Doublet Models*, *Phys.Rev.* **D88** (2013) 015018, [arXiv:1305.1624].

[23] S. Kanemura, H. Yokoya, and Y.-J. Zheng, *Complementarity in direct searches for additional Higgs bosons at the LHC and the International Linear Collider*, *Nucl.Phys.* **B886** (2014) 524–553, [arXiv:1404.5835].

[24] L. Wang and X.-F. Han, *Study of the heavy CP-even Higgs with mass 125 GeV in two-Higgs-doublet models at the LHC and ILC*, *JHEP* **1411** (2014) 085, [arXiv:1404.7437].

[25] G. Dorsch, S. Huber, and J. No, *A strong electroweak phase transition in the 2HDM after LHC8*, *JHEP* **1310** (2013) 029, [arXiv:1305.6610].

[26] J. Shu and Y. Zhang, *Impact of a CP Violating Higgs Sector: From LHC to Baryogenesis*, *Phys.Rev.Lett.* **111** (2013) 091801, [arXiv:1304.0773].

[27] M. Ahmadvand, *Baryogenesis within the two-Higgs-doublet model in the Electroweak scale*, *Int.J.Mod.Phys.* **A29** (2014) 1450090, [arXiv:1308.3767].

[28] G. Dorsch, S. Huber, K. Mimasu, and J. No, *Echoes of the Electroweak Phase Transition: Discovering a second Higgs doublet through $A_0 \to ZH_0$*, *Phys.Rev.Lett.* **113** (2014), no. 21 211802, [arXiv:1405.5537].

[29] A. Drozd, B. Grzadkowski, J. F. Gunion, and Y. Jiang, *Two-Higgs-Doublet Models and Enhanced Rates for a 125 GeV Higgs*, *JHEP* **1305** (2013) 072, [arXiv:1211.3580].

[30] G. Belanger, B. Dumont, U. Ellwanger, J. Gunion, and S. Kraml, *Global fit to Higgs signal strengths and couplings and implications for extended Higgs sectors*, *Phys.Rev.* **D88** (2013) 075008, [arXiv:1306.2941].

[31] A. Arhrib, P. Ferreira, and R. Santos, *Are There Hidden Scalars in LHC Higgs Results?*, *JHEP* **1403** (2014) 053, [arXiv:1311.1520].

[32] **CMS** Collaboration, *Search for extended Higgs sectors in the $H \to hh$ and $A \to Zh$ channels in $\sqrt{s} = 8$ TeV pp collisions with multileptons and photons final states, CMS-PAS-HIG-13-025*, .

[33] D. Eriksson, J. Rathsman, and O. Stal, *2HDMC: Two-Higgs-Doublet Model Calculator Physics and Manual*, *Comput.Phys.Commun.* **181** (2010) 189–205.

[34] D. Eriksson, J. Rathsman, and O. Stal, *2HDMC: Two-Higgs-doublet model calculator*, *Comput.Phys.Commun.* **181** (2010) 833–834.

[35] **CMS** Collaboration, *Higgs to tau tau (MSSM), CMS-PAS-HIG-13-021*, .

[36] **ATLAS** Collaboration, *Measurements of the properties of the Higgs-like boson in the four lepton decay channel with the ATLAS detector using 25 fb1 of proton-proton collision data, ATLAS-CONF-2013-013*, .

[37] *Properties of the Higgs-like boson in the decay $H \to ZZ \to 4\ell$ in pp collisions at $\sqrt{s} = 7$ and 8 TeV*, Tech. Rep. CMS-PAS-HIG-13-002, CERN, Geneva, 2013.

[38] https://twiki.cern.ch/twiki/bin/view/CMSPublic/Hig13002TWiki#Limit_Plot.

[39] *Search for a heavy Higgs boson in the $H \to ZZ \to 2\ell 2nu$ channel in pp collisions at $\sqrt{s} = 7$ and 8 TeV*, Tech. Rep. CMS-PAS-HIG-13-014, CERN, Geneva, 2013.

[40] A. Korytov. private communication.

[41] P. Ferreira, J. F. Gunion, H. E. Haber, and R. Santos, *Probing wrong-sign Yukawa couplings at the LHC and a future linear collider*, *Phys.Rev.* **D89** (2014) 115003, [arXiv:1403.4736].

[42] A. Efrati and Y. Nir, *What if* $\lambda_{hhh} \neq 3m_h^2/v$, arXiv:1401.0935.

[43] S. Dawson, A. Gritsan, H. Logan, J. Qian, C. Tully, et al., *Higgs Working Group Report of the Snowmass 2013 Community Planning Study*, arXiv:1310.8361.

[44] B. Coleppa, F. Kling, and S. Su, *Exotic Decays Of A Heavy Neutral Higgs Through HZ/AZ Channel*, *JHEP* **1409** (2014) 161, [arXiv:1404.1922].